scientific reports

Check for updates

OPEN

Antenna optimization using machine learning with reduced-dimensionality surrogates

Slawomir Koziel[1,2]✉, Anna Pietrenko-Dabrowska[2] & Leifur Leifsson[3]

In modern times, antenna design has become more demanding than ever. The escalating requirements for performance and functionality drive the development of intricately structured antennas, where parameters must be meticulously adjusted to achieve peak performance. Often, global adjustments to geometry are necessary for optimal results. However, direct manipulation of antenna responses evaluated with full-wave electromagnetic (EM) simulation models using conventional nature-inspired methods entails significant computational costs. Alternatively, surrogate-based techniques show promise but are impeded by dimensionality-related challenges and nonlinearity of antenna outputs. This study introduces an innovative technique for swiftly optimizing antennas. It leverages a machine learning framework with an infill criterion employing predicted enhancement of the merit function, utilizing a particle swarm optimizer as the primary search engine, and employs kriging for constructing the underlying surrogate model. The surrogate model operates within a reduced-dimensionality domain, guided by directions corresponding to maximum antenna response variability identified through fast global sensitivity analysis, tailored explicitly for domain determination. Operating within this reduced domain enables building dependable metamodels at a significantly lower computational cost. To address accuracy loss resulting from dimensionality reduction, the global optimization phase is supplemented by local sensitivity-based parameter adjustment. Extensive comparative experiments involving various planar antennas demonstrate the competitive operation of the presented technique over machine learning algorithms operating in full-dimensionality space and direct EM-driven bio-inspired optimization techniques.

Keywords Antennas, EM-based design, Global search, Sensitivity analysis, Surrogate modeling, Nature-inspired algorithms

Designing modern antennas poses a significant challenge. On the one hand, there has been an unprecedented increase in performance demands observed over the recent years, driven by emerging application areas like mobile communications[1], 5G/6G technology[2], internet of things, IoT[3], medical imaging[4], vehicular radars[5], energy harvesting[6], radio-frequency identification[7], etc. On the other hand, antenna systems are expected to provide a number of functionalities (multi-band[8] and MIMO operation[9], pattern diversity[10,11], reconfigurability[12], beam steering[13]), many of which are oriented toward re-use of the same hardware for various operating bands[14], reducing the physical space occupied by the radiators[15]. As a matter of fact, compact size has become one of the most important prerequisites[16–19], resulting in the development of a variety of techniques for the design of electrically small antennas[20–22]. Meeting the aforementioned requirements fosters the development of rather sophisticated structures featuring a number of auxiliary components (slots[23], stubs[24], impedance transformers[25], shorting pins[26]), defected ground structures[27], metamaterial components[28], substrate integrated waveguide (SIW) cavities[29], or multi-layer implementations[30]. Needless to say, with the increase of topological complexity, appropriate tuning of antenna geometry parameters becomes imperative yet intricate. On the one hand, dimension adjustment has to realized using electromagnetic (EM) models to maintain reliability, but also because of the lack of alternatives. For example, equivalent circuit representations often observed in antenna-related works[31,32]

[1]Engineering Optimization and Modeling Center, Reykjavik University, 101 Reykjavík, Iceland. [2]Faculty of Electronics, Telecommunications and Informatics, Gdansk University of Technology, 80-233 Gdańsk, Poland. [3]School of Aeronautics and Astronautics, Purdue University, West Lafayette, IN 47907, USA. ✉email: koziel@ru.is

exhibit no design utility, their role being a sort of post-design illustration of antenna properties. Furthermore, the tuning process has to be simultaneously carried out for a number of parameters, several antenna characteristics, and it is often subject to constraints[33,34].

In engineering practice, antenna parameter tuning is still widely addressed using interactive methods, namely, parametric studies guided by the designer's insight[35,36]. Notwithstanding, yielding optimum designs is contingent upon formal numerical optimization, which are imperative to account for interactions between multiple parameters and accommodate various performance demands. Unfortunately, although a plethora of matured algorithms are available, EM-driven antenna optimization is severely hindered by the associated computational expenses. While the costs of local (e.g., gradient-based) search are typically borderline-acceptable (dozens to hundreds of EM analyses), global optimization[37–39] is typically unmanageable when using the most popular class of metaheuristic algorithms[40–44]. Yet, globalized parameter tuning is often recommended, e.g., for problems that are inherently multimodal (e.g., radiation pattern synthesis of antenna arrays[45,46], design of frequency selective surfaces[47] or coding metasurfaces[48]), development of miniaturized structures[49,50], of when a sufficiently good starting point is unavailable, e.g., antenna re-design for center frequencies considerably misaligned with those at the available design[51].

In contemporary times, bio-inspired population-based methods have become the prevalent choice for global search[52–55]. This class encompasses widely used techniques such as evolutionary algorithms (EAs), evolutionary strategies, genetic algorithms (GAs)[56–58], differential evolution (DE), firefly algorithm, particle swarm optimizers (PSO)[59–61], harmony search[62], grey wolf optimization[37], ant systems[63], and invasive weed optimization[64]. Recently, the proliferation of such methods has been notable (e.g. [65–68].); however, the practical distinctions among these algorithms appear to be minor. The ability to perform global search is typically attributed to the exchange of information between the members of a population undergoing processing by the algorithm, facilitated by recombination and mutation operators (GAs, EAs[56]), or by mimicking social behaviour (or hunting/preying habits)[69], e.g., randomized biasing of design relocation toward locally or globally best solution identified thus far[59]. The downside of bio-inspired methods is their inferior computational efficiency. These algorithms typically need thousands of objective function calls to produce a satisfactory solution. Such costs are often prohibitive when considering direct EM-driven antenna design unless each simulation can be completed swiftly (e.g., within a few seconds) or if there are sufficient resources available for parallelization[70].

A workaround for the aforementioned cost issues has been offered by surrogate modeling techniques[71–73]. In practice, surrogate-assisted frameworks are most often implemented in the form of iterative procedures, where the fast replacement model (kriging[74], neural networks[75], Gaussian process regression[76], etc.) is rendered using EM analysis results garnered during the optimization process and used to yield further approximations of the optimum design[77]. The infill criteria employed in optimization aim at exploring the design variable space (in particular, enhancing the model's accuracy[78]) or exploiting it (identifying the optimal design[79]). Although these methods are often categorized as machine learning algorithms[80–82], the main challenge lies in constructing the surrogate model itself. This challenge is a result of the curse of dimensionality and antenna response nonlinearity. Consequently, surrogate-based bio-inspired methods are typically showcased with relatively simple test cases with only a few independent parameters[83–85]. Various techniques have been developed to address dimensionality issues. Some of these include modeling within constrained domains[86–89] (though applying this concept for global optimization may pose challenges), employing multi-fidelity simulations[90], and utilizing response feature technology[91]. The latter has proven suitable for local optimization[92] as well as surrogate modeling[93]. Feature-based methods involve re-stating the optimization problem using suitably assigned characteristic points of the system outputs and their weakly nonlinear dependence design variables[94]. However, this technique's effectiveness depends on characteristic points over the entire design space.

This research presents an innovative approach to globally tuning antenna parameters at low cost. Our methodology involves a machine learning procedure using the merit function enhancement predicted by the underlying surrogate as the infill criterion and employs a bio-inspired algorithm as the core search engine. The underlying metamodel is developed by means of kriging interpolation and is established within a reduced-dimensionality domain, which is crucial for computational efficiency. This domain is defined using a small number of directions (up to fifty percent of the original design variable space dimensionality) associated with maximum variability in antenna response. We employ a fast global sensitivity analysis (FGSA) technique to identify these domain-defining vectors, custom-developed for domain determination. Unlike traditional GSA approaches, our technique relies on a few random data samples and spectral analysis of antenna response variations extracted from the nearest neighbours of respective points. Operating within this reduced domain permits building dependable metamodels at low cost. Additionally, the global optimization phase is supplemented by local gradient-based tuning to offset any accuracy loss due to dimensionality reduction. We extensively validate our technique using several microstrip antennas and compare it to direct EM-driven nature-inspired optimization, multiple start gradient search, and a machine learning framework operating in full-dimensionality space. The results demonstrate consistent performance across the test case set, competitive outcomes measured by the mean merit function value, and low running costs, averaging only 300 EM evaluations of the antenna under design.

Machine-learning-based global optimization by means of dimensionality-reduced surrogates

In this section, we present the strategy for globally optimizing antenna structures as proposed in this study. Our technique primarily revolves around a machine learning (ML) framework utilizing kriging interpolation surrogates, with a particle swarm optimizer (PSO) being the core optimization procedure. These surrogates are constructed within a reduced-dimensionality domain, established through fast global sensitivity analysis (FGSA). FGSA is specifically designed to swiftly determine the most critical directions in the parameter space on a global

scale. The domain spanned along these directions captures the majority of antenna response variability, while its low dimensionality enables the construction of reliable surrogates using only limited training data samples. The ML search process, guided by the predicted objective function improvement as criterion for infill point generation, is further supplemented by local gradient-based parameter tuning.

The subsequent part of this section is structured as follows: "Design task formulation" section revisits the formulation of the optimization task. Fast regression-based global sensitivity analysis is discussed in "Fast global sensitivity analysis" section, while "Global search stage" section delves into the global search stage. Details of the local tuning algorithm are provided in "Final tuning" section. Finally, the entire procedure is summarized in "Complete optimization procedure" section.

Design task formulation

Meticulous adjustment of parameters is imperative to ensure the best possible operation of antennas. One of the key aspects of this process is appropriate quantification of design quality. This is typically arranged through a scalar cost function, defined so that its lower value are associated with a better design. If several objectives are present, they are typically aggregated (using, e.g., a weighted function approach[95]) or cast into constraints[96].

Figure 1 provides information about the notation utilized in this context. With this terminology, the simulation-driven antenna optimization task can be posed as

$$\boldsymbol{x}^* = \arg\min_{\boldsymbol{x}\in X} U(\boldsymbol{x}) \tag{1}$$

here $\boldsymbol{x}^*$ stands for the optimum parameter vector. Antenna responses are evaluated by means of EM simulation.

More often than not, there are constraints imposed upon task (1) denoted as g_k (inequality conditions) and h_k (equality conditions), cf. Figure 1. Constraint handling may be implicit[96], where the problem (1) is re-stated as

$$\boldsymbol{x}^* = \arg\min_{\boldsymbol{x}} U_P(\boldsymbol{x}) \tag{2}$$

In (2), U_P is composed of the cost function U and the penalty functions. We have

$$U_P(\boldsymbol{x}) = U(\boldsymbol{x}) + \sum_{k=1}^{n_g+n_h} \beta_k c_k(\boldsymbol{x}) \tag{3}$$

where $c_k(\boldsymbol{x})$ evaluate constraint violations, while coefficients β_k control the impact of penalty terms on U_P.

Figure 2 illustrates various scenarios of antenna design optimization. It is worth noting that the penalty functions depicted therein account for the relative constraint violation concerning the assumed acceptance level (e.g., – 10 dB for $|S_{11}|$). Utilizing the second power ensures that U_P becomes a differentiable function of constraint violation at the boundary of the feasible region, thereby facilitating its exploration. The latter is crucial because one or more constraints are typically active at the optimal design. The frequency spectrum F of interest may constitute a single continuous range of frequencies for a single-band antenna, particularly for broadband antennas, i.e., $F = [f_1\, f_2]$, or it may represent a number of target operating frequency ranges for a multi-band antenna, i.e., $F = [f_{1.1} f_{1.2}] \cup [f_{2.1} f_{2.2}] \cup \cdots \cup [f_{N.1} f_{N.2}]$, where N is a number of bands.

Fast global sensitivity analysis

The global search algorithm introduced in this study relies on data-driven surrogate models. The major bottleneck of behavioural modelling of antenna structures is a combined effect of the parameter space dimensionality, nonlinearity of antenna outputs, but also wide ranges of design variables. Dimensionality reduction is a key factor that may facilitate the construction of reliable surrogates at reasonable computational expenses.

Symbol	Meaning	Comments
$\boldsymbol{x} = [x_1 \ldots x_n]^T$	Designable parameters	Typically, antenna dimensions expressed in mm
$X = [\boldsymbol{l}\ \boldsymbol{u}]$	Parameter space	Parameter space is normally determined using lower and upper bounds on design parameters $\boldsymbol{l} = [l_1 \ldots l_n]^T$, and $\boldsymbol{u} = [u_1 \ldots u_n]^T$
$U(\boldsymbol{x})$	Objective (merit) function	The function U determines the design quality; it is defined so that better designs correspond to lower values of U
$g_k(\boldsymbol{x}) \le 0$, $k = 1, \ldots, n_g$	Inequality constraints	Typically, constraints defined by imposing lower or upper acceptance thresholds for specific antenna responses over selected frequency ranges
$h_k(\boldsymbol{x}) = 0$, $k = 1, \ldots, n_h$	Equality constraints	Typically, constraints defined by imposing specific target values for selected operating figures (e.g., resonant frequency) of the antenna

Fig. 1. Antenna optimization: notation and terminology.

Design scenario: verbal description	Objective function (1) and constraints	Objective function (3)
Design for best in-band matching within the frequency range F	$U(\boldsymbol{x}) = S(\boldsymbol{x}) = \max\{f \in F : \lvert S_{11}(\boldsymbol{x},f)\rvert\}$	$U_P(\boldsymbol{x}) = U(\boldsymbol{x})$
Design for maximum average in-band gain (in frequency range F); ensuring that in-band matching does not exceed –10 dB in F	$U(\boldsymbol{x}) = \bar{G}(\boldsymbol{x}) = \frac{1}{F}\int_F G(\boldsymbol{x},f)df$ Constraint: $\lvert S_{11}(\boldsymbol{x},f)\rvert \le -10$ dB for $f \in F$	$U_P(\boldsymbol{x}) = \bar{G}(\boldsymbol{x}) + \beta_1 c_1(\boldsymbol{x})^2$ where $c_1(\boldsymbol{x}) = \left[\frac{\max(S(\boldsymbol{x})+10,0)}{10}\right]^2$
Design for minimum in-band axial ratio (in frequency range F); ensuring that in-band matching does not exceed –10 dB in F	$U(\boldsymbol{x}) = A_R(\boldsymbol{x}) = \max\{f \in F : AR(\boldsymbol{x},f)\}$ Constraint: $\lvert S_{11}(\boldsymbol{x},f)\rvert \le -10$ dB for $f \in F$	$U_P(\boldsymbol{x}) = A_R(\boldsymbol{x}) + \beta_1 c_1(\boldsymbol{x})^2$ where $c_1(\boldsymbol{x}) = \left[\frac{\max(S(\boldsymbol{x})+10,0)}{10}\right]^2$
Design for size reduction of a circularly polarized antenna; ensuring that in-band matching (in frequency range F) does not exceed –10 dB, and axial ratio does not exceed 3 dB	$U(\boldsymbol{x}) = A(\boldsymbol{x})$ Constraints: $AR(\boldsymbol{x},f) \le 3$ dB for $f \in F$ and $\lvert S_{11}(\boldsymbol{x},f)\rvert \le -10$ dB for $f \in F$	$U_P(\boldsymbol{x}) = A(\boldsymbol{x}) + \beta_1 c_1(\boldsymbol{x})^2 + \beta_2 c_2(\boldsymbol{x})^2$ where $c_1(\boldsymbol{x}) = \left[\frac{\max(S(\boldsymbol{x})+10,0)}{10}\right]^2$ and $c_2(\boldsymbol{x}) = \left[\frac{\max(A_R(\boldsymbol{x})-3,0)}{3}\right]^2$

Explanation of terms:
- f – frequency,
- $\lvert S_{11}(\boldsymbol{x},f)\rvert$ – modulus of the reflection coefficient at design $\boldsymbol{x}$ and frequency f,
- $G(\boldsymbol{x},f)$ – realized gain,
- $AR(\boldsymbol{x},f)$ – axial ratio,
- $A(\boldsymbol{x})$ – antenna size (e.g., footprint area).

Fig. 2. Examples of parameter tuning scenarios for antenna structures.

In the realm of global search, the approaches available in the literature include variable screening (e.g., Pearson correlation coefficients[97], partial correlation coefficients[98], Morris method[99]), but also global sensitivity analysis (GSA), e.g., Sobol indices[100], regression-based methods[101], or Jansen method[102]. The purpose of these methods is to determine relative impact of the specific parameters, which allows the user to exclude those that are of minor significance. However, the majority of the mentioned approaches are costly, i.e., entail large number of samples, required to evaluate the sensitivity indicators. Furthermore, in antenna design, the exclusion of individual variables is usually not advisable because most of geometry parameters affect antenna responses through combined effects with other parameters. This prompts to the development of an alternative GSA approach, which is to satisfy the following conditions:

- Low computational cost (e.g., less than a hundred EM simulations);
- The ability to determine essential directions in the design variable space that are of importance from the perspective of their effects on antenna characteristics, rather than to identify individual parameters.

In the following, we will provide the outline and elucidate the details of the proposed fast GSA (referred to as FGSA) developed to comply with the aforementioned conditions.

Fast global sensitivity analysis

Figure 3 shows the operating flow of the fast GSA technique (referred to as FGSA). Spectral analysis of the relocation matrix $\boldsymbol{S}$ yields the eigenvectors $\boldsymbol{e}_j$, representing the parameter space directions that have decreasing effects on the antenna response variability. The importance of particular directions in the above sense is quantified using the corresponding eigenvalues λ_j. The vectors $\boldsymbol{e}_j$, $j = 1, \ldots, n$, constitute an orthonormal basis in the design variable space X.

The outcome of FGSA will allow us to define a reduced-dimensionality domain of the metamodel, which will be used in the global optimization phase of our algorithm, cf. "Global search stage" section. The domain is determined by a few essential eigenvectors. Their number is determined as the smallest integer $N_d \in \{1, 2, \ldots, n\}$ that satisfies

$$\frac{\sqrt{\sum_{j=1}^{N_d} \lambda_j^2}}{\sqrt{\sum_{j=1}^{n} \lambda_j^2}} \ge C_{\min}. \tag{8}$$

According to (8), N_d is the minimum number of vectors for which the overall (relative) least-square antenna response variability exceeds the user-defined threshold $C_{\min}$. For the sake of verification experiments described

1. Input parameters:
   - Parameter space X;
   - Computational model $\boldsymbol{R}(\boldsymbol{x})$;
   - Number of samples N_s;
2. Generate N_s random vectors $\boldsymbol{x}_s^{(k)} \in X$, $k = 1, \ldots, N_s$, preferably in a uniform manner. Here, we use modified Latin Hypercube Sampling (LHS)[104];
3. Acquire EM simulation data $\boldsymbol{R}(\boldsymbol{x}_s^{(k)})$, $k = 1, \ldots, N_s$;
4. For each $k = 1, \ldots, N_s$, find $\boldsymbol{x}_c^{(k)} = \boldsymbol{x}_s^{(j\min)}$ such that
$$j_{\min} = \arg \min_{\substack{1 \le j \le N_s \\ j \ne k}} \left\| \boldsymbol{x}_s^{(k)} - \boldsymbol{x}_s^{(j)} \right\| \tag{4}$$
In other words, $\boldsymbol{x}_c^{(k)}$ is the vector closest to $\boldsymbol{x}_s^{(k)}$ in the norm sense;
5. Compute (normalized) relocation vectors
$$\boldsymbol{v}_s^{(k)} = \frac{\boldsymbol{x}_c^{(k)} - \boldsymbol{x}_s^{(k)}}{\left\| \boldsymbol{x}_c^{(k)} - \boldsymbol{x}_s^{(k)} \right\|} \tag{5}$$
and the corresponding (normalized) response variabilities
$$r_s^{(k)} = \frac{\boldsymbol{R}(\boldsymbol{x}_c^{(k)}) - \boldsymbol{R}(\boldsymbol{x}_s^{(k)})}{\left\| \boldsymbol{x}_c^{(k)} - \boldsymbol{x}_s^{(k)} \right\|} \tag{6}$$
for $k = 1, \ldots, N_s$;
6. Define a $N_s \times n$ relocation matrix $\boldsymbol{S}$ as
$$\boldsymbol{S} = \begin{bmatrix} r_s^{(1)} (\boldsymbol{v}_s^{(1)})^T \\ \vdots \\ r_s^{(N_s)} (\boldsymbol{v}_s^{(N_s)})^T \end{bmatrix} \tag{7}$$
The rows of $\boldsymbol{S}$ represent relocation vectors normalized with respect to their importance in terms of how they affect the circuit response in the norm sense;
7. Perform spectral analysis of $\boldsymbol{S}$[105] in order to find its eigenvectors $\boldsymbol{e}_j$ (principal components) and the corresponding eigenvalues λ_j, $j = 1, \ldots, n$. The eigenvalues are ordered, so that $\lambda_1 \ge \lambda_2 \ge \ldots \lambda_n$.

Fig. 3. Pseudocode of the proposed fast global sensitivity analysis (FGSA). The eigenvectors $\boldsymbol{e}_j$ represent the parameter space directions having major effects on antenna responses; the importance is quantified using the eigenvalues λ_j[103,104].

in "Verification experiments" section, we set $C_{\min} = 0.9$, i.e., it is assumed that the domain-defining directions should account for at least ninety percent of the overall response variability.

Examples To illustrate FGSA, let us consider a few examples, starting from a linear function $f(\boldsymbol{x}) = f([x_1\ x_2]^T) = 3x_1 - 2x_2$, shown in Fig. 4. Linearity of f allows us to immediately identify the direction of maximum variability, which is the gradient $\boldsymbol{g} = [3 - 2]^T$. Applying FGSA with twenty random observables leads to the same result (cf. Figure 4b). Two additional examples have been shown in Fig. 5. These are also arranged to allow visual assessment of the direction of maximum variability (as the vector perpendicular to the function 'ripples'), which is confirmed using FGSA, again, executed using twenty random observables.

The final example is an antenna illustrated in Fig. 6a. The design variable space contains ten parameters, $\boldsymbol{x} = [l_1 l_2 l_{3r} l_4 l_{5r} w_1 w_2 w_3 w_4 w_5]^T$. The FGSA procedure has been executed using fifty random observables uniformly allocated in $X = [\boldsymbol{l}\ \boldsymbol{u}]^T$, which is a set delimited by the bounds $\boldsymbol{l} = [20.0\ 3.0\ 0.6\ 3.0\ 0.6\ 0.5\ 2.5\ 0.5\ 2.5\ 0.5]^T$, and $\boldsymbol{u} = [50.0\ 5.0\ 0.85\ 5.0\ 0.85\ 1.5\ 3.5\ 1.5\ 3.5\ 1.5]^T$.

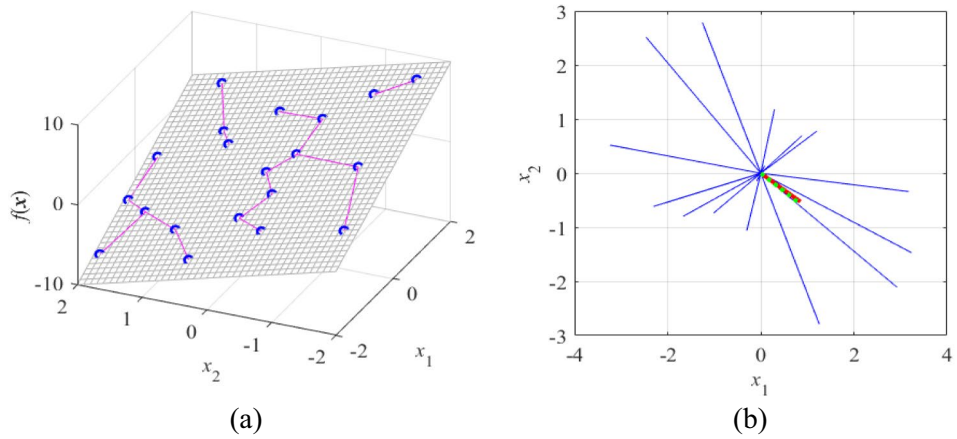

Fig. 4. FGSA illustration using a linear function $f(\boldsymbol{x}) = f([x_1\ x_2]^T) = 3x_1 - 2x_2$: (**a**) surface plot of the function (gray), twenty random observables $\boldsymbol{x}_s^{(k)}$ (circles), and relocation vectors $\boldsymbol{x}_c^{(k)} - \boldsymbol{x}_s^{(k)}$ (line segments); (**b**) relocation matrix vectors $r_s^{(k)}\boldsymbol{v}_s^{(k)}$ (thin lines), the largest principal component $\boldsymbol{e}_1$ (thick solid line), and the normalized gradient $\boldsymbol{g} = [3\ -2]^T/13^{1/2}$ (thick dotted line). In this example, all function variability occurs along the gradient $\boldsymbol{g}$ (the function is constant in the direction orthogonal to $\boldsymbol{g}$), which is well aligned with the vector $\boldsymbol{e}_1$, obtained using the proposed FGSA.

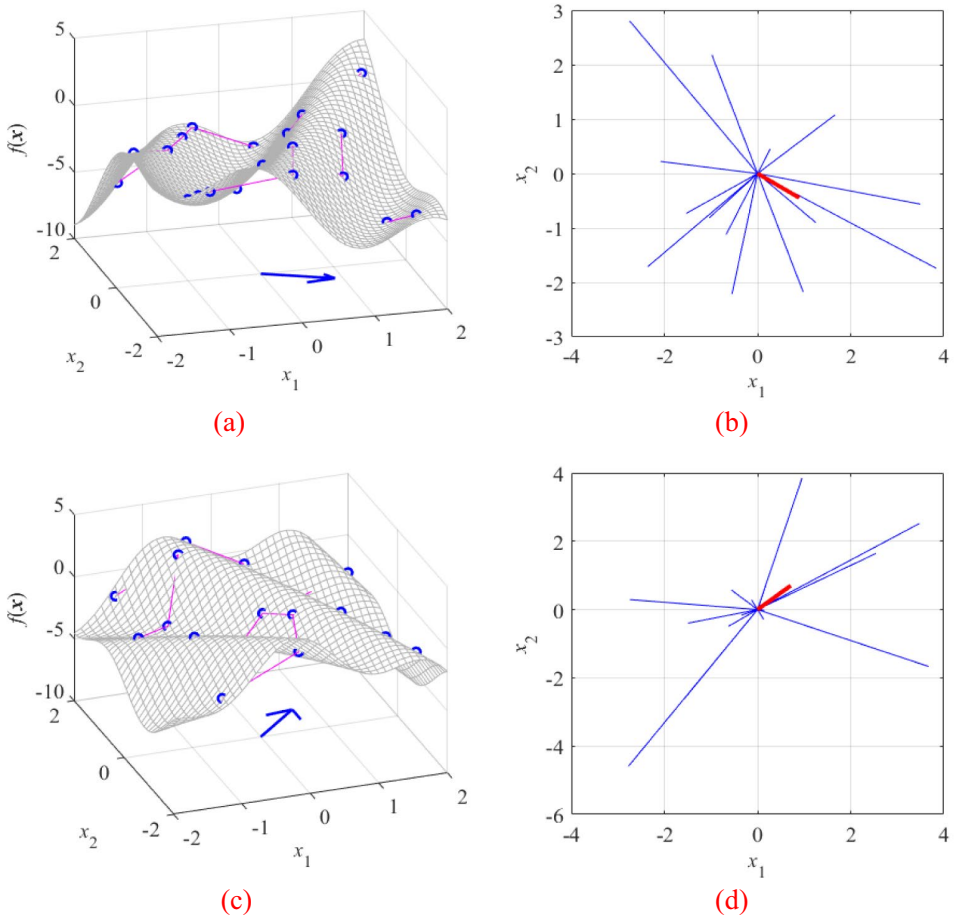

Fig. 5. FGSA illustration using nonlinear functions of two variables: (**a**) surface plot of the first function (gray), twenty random observables $\boldsymbol{x}_s^{(k)}$ (circles), and relocation vectors $\boldsymbol{x}_c^{(k)} - \boldsymbol{x}_s^{(k)}$ (line segments), as well as the principal component $\boldsymbol{e}_1$ (thick arrow); (**b**) relocation matrix vectors $r_s^{(k)}\boldsymbol{v}_s^{(k)}$ (thin lines), and the largest principal component $\boldsymbol{e}_1$ (thick solid line); (**c**) and (**d**) surface plot and relocation matrix vectors for the second function. It can be noticed that the vector $\boldsymbol{e}_1$ obtained using FGSA visually corresponds to the direction of the largest variability of the function $f(\boldsymbol{x})$.

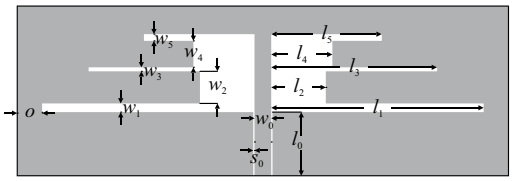

(a)

j	1	2	3	4	5	6	7	8	9	10
λ_j	1.00	0.67	0.54	0.43	0.40	0.32	0.24	0.23	0.19	0.13
dR_j	1.00	0.76	0.52	0.46	0.25	0.40	0.29	0.26	0.25	0.19

(b)

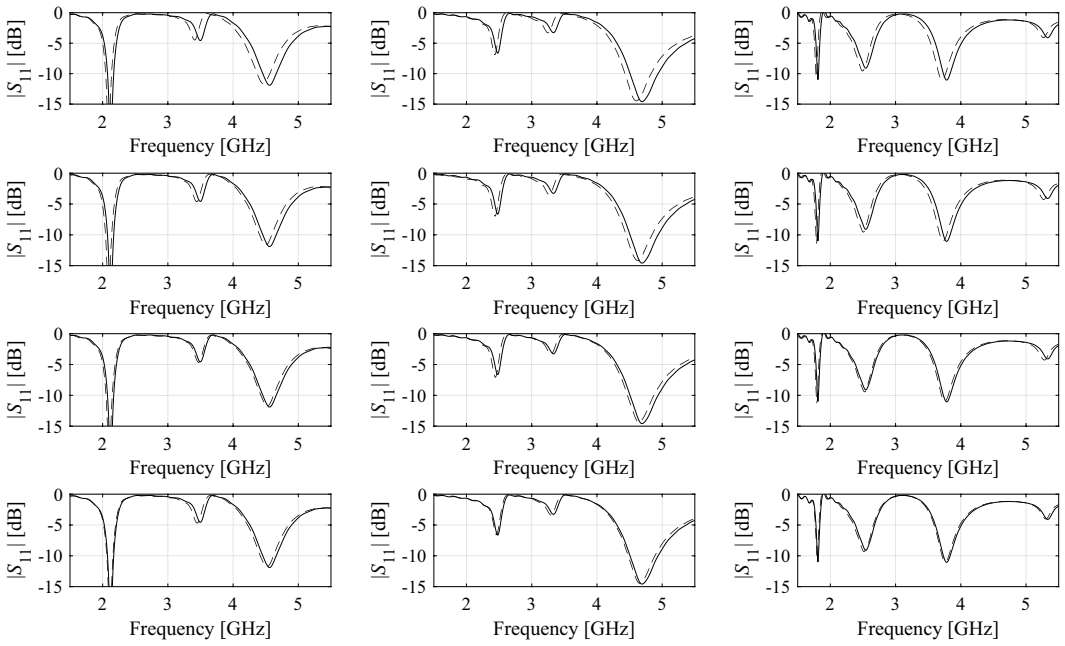

(c)

Fig. 6. FGSA illustration using a triple-band dipole: (**a**) antenna architecture; the antenna is implemented by etching the slots (shown white) in the upper metallization (gray). The structure is realized on a dielectric substrate of thickness 0.76 mm (cf. Table 2 for more details); (**b**) normalized eigenvalues of the relocation matrix $\boldsymbol{S}$ obtained using FSGA based on fifty random samples, as well as average EM-simulated variability indicators dR_j computed as in (9); (**c**) reflection responses at three random designs (left, middle, and right panels), and designs perturbed along the first four principal components, $\boldsymbol{x}+h\boldsymbol{e}_k$ with $h=0.1$ (from top to bottom) obtained using FGSA. Responses at design $\boldsymbol{x}$ shown as solid line, responses at perturbed design shown using dashed lines. It can be observed that response variability is gradually reduced for increasing k, which demonstrates that subsequent eigenvectors correspond to directions having less and less effect on antenna characteristics.

The EM-evaluated reflection characteristics have been illustrated in Fig. 6c for several randomly-selected parameter vector $\boldsymbol{x}^{(j)}$, $j=1, \ldots, 4$, and designs perturbed along the eigenvectors $\boldsymbol{e}_k$, i.e., $\boldsymbol{x}^{(j)}+h\boldsymbol{e}_k$, $k=1, \ldots, n$. As expected, on the average, the response variability is the largest for $k=1$, and it is gradually reduced for increasing k.

The actual response variability was estimated using $N_r=50$ random designs, $\boldsymbol{x}_r^{(k)}$, $k=1, \ldots, N_r$, along with the perturbations $\boldsymbol{x}_r^{(k,j)}=\boldsymbol{x}_r^{(k)}+h\boldsymbol{e}_j$, $j=1, \ldots, n$. Using the EM simulation data $\boldsymbol{R}(\boldsymbol{x}_r^{(k)})$, $k=1, \ldots, N_r$, and $\boldsymbol{R}(\boldsymbol{x}_r^{(k,j)})$, $k\in\{1, \ldots, N_r\}$, $j\in\{1, \ldots, n\}$, the response variability factors were obtained as

$$dR_j = \frac{1}{N_r}\sum_{k=1}^{N_r}\left\|\mathbf{R}_f\left(\mathbf{x}_r^{(k)}\right)-\mathbf{R}_f\left(\mathbf{x}_r^{(k\cdot j)}\right)\right\| \tag{9}$$

for $j=1, \ldots, n$. Note that dR_j stand for the average response variability along the eigenvector $\boldsymbol{e}_j$. Normalized values of dR_j agree well with the normalized eigenvalues λ_j, as indicated in Fig. 6b. This, again, demonstrates the relevance of FGSA.

The principal benefit of FGSA is its efficacy. As mentioned earlier, most of global sensitivity analysis techniques (e.g., Sobol indices[100], regression-based methods[101]), while offering a better accuracy, require much larger datasets, often ranging from hundreds to even thousands of samples. FGSA is executed with only a few dozen observables. Another advantage of this technique is its ability to identify principal directions that are arbitrarily allocated (i.e., do not have to coincide with the coordinate system axes). The latter allows exploring joint parameter effects on antenna responses, rather than eliminating individual parameters.

It should be emphasized that FGSA allows us to evaluate the average effects of particular parameter space directions on the antenna responses. These may slightly change in various parts of the parameter space. However, quantification of the average effect is exactly what we need because the purpose of FGSA is dimensionality reduction for global optimization. Furthermore, for most antenna structures, the changes of specific parameters (or combinations thereof) have similar effect on antenna responses regardless of a particular design. For example, adjusting a slot size in the dual- or triple-band antennas affect one of the resonant frequencies in a similar way (i.e., if shortened, the frequency is increased, cf. "Verification experiments" section).

Dimensionality-reduced model domain

FGSA aims to identify N_d directions within space X, which are essential in terms of their effects on antenna response variability. These directions (eigenvectors $\boldsymbol{e}_j$, $j = 1, \ldots, N_d$) are used here to define the dimensionality-reduced region X_d. The set X_d serves as a region of validity of the fast metamodel constructed to predict the antenna responses therein. The same region will also be used as a search domain for the global optimization stage.

The set X_d is defined as

$$X_d = \left\{ \mathbf{x} \in X : \mathbf{x} = \mathbf{x}_c + \sum_{j=1}^{N_d} a_j \mathbf{e}_j \right\} \cap X. \tag{10}$$

Thus, X_d is an intersection of the original domain X and the set of vectors $\boldsymbol{x}_c + a_1\boldsymbol{e}_1 + \ldots + a_{Nd}\boldsymbol{e}_{Nd}$, where $\boldsymbol{x}_c = [\boldsymbol{l} + \boldsymbol{u}]/2$ is the center of X, and a_j, $j = 1, \ldots, N_d$, are real numbers. Figure 7 provides a conceptual illustration of X_d.

Reducing dimensionality is essential for the accuracy of the surrogate (here, rendered as a kriging interpolation model[78]). In particular, as $\dim(X_d) = N_d < n$, a usable metamodel can be built with the use of a amount of training data. Reducing the training set carried over to improved efficiency of the search process. Meanwhile, the surrogate's region of validity encapsulates directions that are significant for the antenna response variability, thereby ensuring its design utility.

Global search stage

The first (global) optimization stage incorporates two steps. It is commenced by constructing an initial surrogate model within domain X_d determined using the procedure explained in "Dimensionality-reduced model domain" section. Subsequently, a machine learning process is launched, by means of which the globally optimum design is sought for. In each iteration of this process, the PSO algorithm yields the next (infill) point by minimizing surrogate-predicted objective function. Meanwhile, the surrogate itself is refined based on the accumulated EM simulation data. These two steps are elucidated in "Initial surrogate" and "Machine-learning-based global optimization" sections.

Initial surrogate

The first surrogate is established in the reduced-dimensionality region X_d using kriging[78]. The kriging model setup is as follows: (i) second-order polynomial as a trend function, (ii) Gaussian correlation functions $R(\boldsymbol{h}) = \exp(-\Sigma_{j=1,\ldots,n} h_j\theta_j)$, where $\boldsymbol{h} = [h_1 \ldots h_n]^T$, and θ_j are the model's hyperparameters. The training dataset size is N_iN_d, where N_i is the user-defined multiplier (here, set to $N_i = 20$). The samples $\boldsymbol{x}_B^{(k)}$, $k = 1, \ldots, N_iN_d$, are allocated uniformly in X_d, and the model $\boldsymbol{s}_{tmp}(\boldsymbol{x})$ is constructed using the dataset $\{\boldsymbol{x}_B^{(k)}, \boldsymbol{R}(\boldsymbol{x}_B^{(k)})\}_{k = 1, \ldots, NiNd}$, with the antenna responses $\boldsymbol{R}(\boldsymbol{x}_B^{(k)})$ acquired using EM analysis. Subsequently, the infill points are generated by increasing the mean square error (MSE) predicted by the current surrogate model

$$\mathbf{x}_B^{(N_iN_d+j)} = \arg\max_{\mathbf{x} \in X_d} MSE(\mathbf{s}_{tmp}(\mathbf{x})) \tag{11}$$

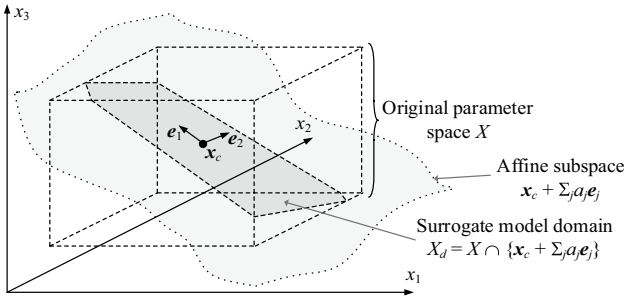

Fig. 7. Reduced-dimensionality domain X_d. Here, the original parameter space is three dimensional, whereas X_d is determined by two eigenvectors $\boldsymbol{e}_1$ and $\boldsymbol{e}_2$. Note that X_d is a set theory intersection of X and the affine subspace $\boldsymbol{x}_c + \Sigma_{j=1,2}\, a_j\boldsymbol{e}_j$.

for $j = 1, 2, \ldots$. The model refined based on the extended training set $\{\boldsymbol{x}_B^{(k)}, \boldsymbol{R}(\boldsymbol{x}_B^{(k)})\}_{k = 1, \ldots, NiNd + j}$, until the cross-validated[105] relative RMS error falls below the user-defined threshold $E_{\max}$, or the total number of samples exceeds $2N_iN_d$ (maximum computational budget).

This arrangement places new training samples in locations corresponding to the maximum predicted model error, which improves the surrogate's global accuracy over the domain X_d. Upon the conclusion of this stage, the current model $\boldsymbol{s}_{tmp}(\boldsymbol{x})$ becomes the initial surrogate $\boldsymbol{s}^{(0)}(\boldsymbol{x})$. The process of constructing the initial metamodel has been depicted in Fig. 8.

Machine-learning-based global optimization

The global optimization stage is a machine learning framework utilizing the initial model $\boldsymbol{s}^{(0)}$ obtained using the guidelines elucidated in "Global search stage" section and the subsequent surrogates $\boldsymbol{s}^{(j)}$, $j = 1, 2, \ldots$, constructed from the EM data acquired in the process.

The parameter vector $\boldsymbol{x}^{(i+1)}$ is generated for $i = 0, 1, 2, \ldots$, by solving the nonlinear minimization task

$$\boldsymbol{x}^{(i+1)} = \arg\min_{\boldsymbol{x} \in X_d} U_S\left(\boldsymbol{x}, \boldsymbol{s}^{(i)}(\boldsymbol{x})\right). \tag{12}$$

The function U_S in (12) has the same analytical form as elucidated in "Design task formulation" section. The subscript S is used to indicate the dependence of U_S on the metamodel $\boldsymbol{s}^{(i)}(\boldsymbol{x})$, which is used instead of EM analysis when solving (12).

A solution to (12) is obtained in a global sense over the surrogate model domain X_d by means of PSO[106], which is perhaps the most widely used bio-inspired routine in engineering. Nevertheless, the particular algorithm choice is of little importance as (12) is straightforward to handle because of the low evaluation cost of $U_S(\boldsymbol{x}, \boldsymbol{s}^{(i)}(\boldsymbol{x}))$. In particular, the CPU cost of solving (12) can be neglected when compared with EM analysis of the underlying antenna structure, even if PSO operating under a large computational budget (e.g., 10,000 objective function evaluations or so).

It should be emphasized that the formulation (12) is equivalent to using the predicted merit function improvement as an infill criterion[107]. The parameter vectors $\boldsymbol{x}^{(i)}$ generated by (12) approximate the optimum design. Furthermore, they are employed to refine the surrogate model. More specifically, the model $\boldsymbol{s}^{(i)}(\boldsymbol{x})$ is rendered using the dataset $\{\boldsymbol{x}_B^{(k)}, \boldsymbol{R}(\boldsymbol{x}_B^{(k)})\}_{k = 1, \ldots, 2NiNd + i}$, where $\boldsymbol{x}_B^{(2NiNd+i)} = \boldsymbol{x}^{(i)}$ for $i = 1, 2, \ldots$.

The termination criteria for the global search phase are as follows (treated as a logical alternative): (i) $||\boldsymbol{x}^{(i+1)} - \boldsymbol{x}^{(i)}|| < \varepsilon$ (convergence in argument), (ii) no improvement of the EM-evaluated merit function over the last $N_{no\_improve}$ iterations. The control parameters are set to $\varepsilon = 10^{-2}$ and $N_{no\_improve} = 20$ in the validation part of the paper ("Verification experiments" section).

Final tuning

The parameter vector produced during the global optimization phase is further enhanced through local parameter tuning over the original design variable space X. This is to ensure that a truly optimum design is found. Recall that global optimization is performed in the dimensionality-reduced domain X_d, which, although defined to cover the most important directions within X, does not account for the entire space.

Here, the specific routine is the trust-region (TR) algorithm[108], recalled below. The TR procedure solves the problem (1), $\boldsymbol{x}^* = \arg\min_{\boldsymbol{x} \in X} U(\boldsymbol{x})$, over the original space X. It works iteratively by generating subsequent approximations to $\boldsymbol{x}^*$, marked as $\boldsymbol{x}^{(i)}$, $i = 0, 1, \ldots$ The design $\boldsymbol{x}^{(i+1)}$ is obtained as

1. Input parameters:
   - Reduced-dimensionality domain X_d (cf. Dimensionality-reduced model domain);
   - Modelling error threshold $E_{\max}$;
   - Initial number of training samples N_iN_d (N_i is the user-defined parameter, N_d is the dimensionality of the reduced domain X_d).
2. Generate $N_i n$ samples $\boldsymbol{x}_B^{(k)} \in X_d$, $k = 1, \ldots, N_iN_d$, using uniform probability distribution;
3. Set $j = 0$;
4. Evaluate antenna responses $\boldsymbol{R}(\boldsymbol{x}_B^{(k)})$, $k = 1, \ldots, N_iN_d + j$, using EM simulation;
5. Construct surrogate model $\boldsymbol{s}_{tmp}(\boldsymbol{x})$ using dataset $\{\boldsymbol{x}_B^{(k)}, \boldsymbol{R}(\boldsymbol{x}_B^{(k)})\}_{k = 1, \ldots, NiNd + j}$;
6. Estimate model error E_{tmp} using K-fold cross-validation[106], $K = \min\{j, 10\}$;
7. **if** $E_{tmp} < E_{\max}$ OR $j > 2N_iN_d$
   Go to 12;
   end
8. Find an infill point by maximizing the mean square error (MSE) of the current surrogate model:
   $$\boldsymbol{x}_B^{(N_iN_d+j)} = \arg\max_{\boldsymbol{x} \in X_d} MSE(\boldsymbol{s}_{tmp}(\boldsymbol{x}))$$
9. Set $j = j + 1$;
10. Evaluate antenna response $\boldsymbol{R}(\boldsymbol{x}_B^{(NiNd+j)})$ using EM simulation;
11. Go to 5;
12. Return $\boldsymbol{s}^{(0)}(\boldsymbol{x}) = \boldsymbol{s}_{tmp}(\boldsymbol{x})$;

Fig. 8. Initial surrogate model construction.

$$\boldsymbol{x}^{(i+1)} = \arg\min_{\boldsymbol{x};\,\|\boldsymbol{x}-\boldsymbol{x}^{(i)}\|\le d^{(i)}} U_L\left(\boldsymbol{x}, \boldsymbol{L}^{(i)}(\boldsymbol{x})\right) \tag{13}$$

where $\boldsymbol{L}^{(i)}(\boldsymbol{x}) = \boldsymbol{R}(\boldsymbol{x}^{(i)}) + \boldsymbol{J}_{\boldsymbol{R}}(\boldsymbol{x}^{(i)})\cdot(\boldsymbol{x}-\boldsymbol{x}^{(i)})$ is a linear approximation model of $\boldsymbol{R}$ at the current iteration point $\boldsymbol{x}^{(i)}$. The function $U_L^{(i)}$ coincides with U yet it is computed based on $\boldsymbol{L}^{(i)}(\boldsymbol{x})$ rather than directly EM-simulated antenna responses $\boldsymbol{R}(\boldsymbol{x})$. This is emphasized by explicitly indicating the dependence of U_L on $\boldsymbol{L}^{(i)}(\boldsymbol{x})$. The size parameter $d^{(i)}$ is modified based using conventional rules[108]. The algorithm is stopped either if $||\boldsymbol{x}^{(i+1)} - \boldsymbol{x}^{(i)}|| < \varepsilon_{TR}$, or if $d^{(i)} \le \varepsilon_{TR}$, whichever occurs first. The user-defined parameter ε_{TR} is a control variable of the algorithm (here, set to $\varepsilon_{TR} = 10^{-3}$).

The antenna response Jacobian $\boldsymbol{J}_{\boldsymbol{R}}(\boldsymbol{x}^{(i)})$ is estimated by means of finite differentiation (FD)[109] during the initial iterations. The associated cost is n EM analyses. When $||\boldsymbol{x}^{(i+1)} - \boldsymbol{x}^{(i)}|| \le 10\varepsilon_{TR}$, i.e., the process approaches convergence, FD is replaced by a Broyden update[110]. Therein, the matrix $\boldsymbol{J}_{\boldsymbol{R}}$ is updated using information about the design relocation and antenna response at the latest iteration[111]:

$$\boldsymbol{J}_{\boldsymbol{R}}^{(i+1)} = \boldsymbol{J}_{\boldsymbol{R}}^{(i)} + \frac{\left(\boldsymbol{f}^{(i+1)} - \boldsymbol{J}_{\boldsymbol{R}}^{(i)} \cdot \boldsymbol{h}^{(i+1)}\right) \cdot \boldsymbol{h}^{(i+1)T}}{\boldsymbol{h}^{(i+1)T}\boldsymbol{h}^{(i+1)}}, \quad i = 0, 1, \ldots \tag{14}$$

where $\boldsymbol{f}^{(i+1)} = \boldsymbol{R}\left(\boldsymbol{x}^{(i+1)}\right) - \boldsymbol{R}\left(\boldsymbol{x}^{(i)}\right)$, and $\boldsymbol{h}^{(i+1)} = \boldsymbol{x}^{(i+1)} - \boldsymbol{x}^{(i)}$. This enables considerable computational savings as evaluation of (14) does not involve EM analysis.

Complete optimization procedure

The global search procedure suggested in this study utilizes the algorithmic component introduced in "Fast global sensitivity analysis" and "Global search stage" sections: fast global sensitivity analysis (FGSA), surrogate modelling using kriging, surrogate-assisted machine learning framework, as well as local parameter tuning using the trust-region algorithm.

The control variables of the presented algorithm have been collected in Table 1. The meaning and the default values of these parameters were already discussed in the previous parts of the paper. It should be emphasized that apart from the parameters related to the termination condition (ε, $N_{no\_improve}$, ε_{TR}), which permits adjustment of the search process resolution, there are only three control variables: N_r, N_i, and $E_{\max}$.

None of them is critical. On the one hand, changing the number of random observables for FGSA does not have a dramatic effect on the sensitivity analysis outcome as the effects of particular parameter space directions are averaged over the parameter space. On the other hand, N_i and $E_{\max}$ are only used for initial surrogate model rendition, which is subsequently refined within the machine learning optimization loop. This means that the algorithm does not require tuning for any specific problem. To demonstrate this feature, identical setup will be used (as specified in the last column of Table 1) for validation experiments discussed in "Verification experiments" section.

Figures 9 and 10 showcase the operating steps and the flow diagram of the proposed methodology. The major steps include global sensitivity analysis (Step 2), determination of the model's domain and initial model rendition (Steps 3 and 4), machine learning global search stage (Steps 6 through 10), and local parameter tuning (Step 12). Global optimization involves iterative generation of the candidate designs as well as surrogate model refinement using the EM data garnered during the search process.

Verification experiments

The global search procedure presented in "Machine-learning-based global optimization by means of dimensionality-reduced surrogates" section is showcased with the help of four planar antennas. These antennas are optimized for various case-dependent scenarios, including matching improvement at target operating frequencies, matching improvement over a continuous frequency spectrum, and maximization of in-band gain. Our framework's performance is juxtaposed against bio-inspired optimization (specifically, PSO), multiple-start gradient-based search, and a machine-learning procedure operating in the original parameter space. The key performance factors include design quality, dependability of the optimization process, and its cost efficiency. The remaining

Parameter	Meaning	Default value
N_r	Number of random observables for fast global sensitivity analysis (FGSA), cf. "Fast global sensitivity analysis" section	50
N_i	Multiplier for the number of uniformly-distributed data samples for initial surrogate model construction; the actual number of samples is $N_i N_d$, with N_d being the dimensionality of the reduced domain X_d (cf. "Initial surrogate" section)	20
$E_{\max}$	Maximum value of relative RMS error of the initial surrogate model (error estimated using cross-validation)	20%
ε	Termination threshold for convergence in argument, cf. "Machine-learning-based global optimization" section	10^{-2}
$N_{no\_improve}$	Termination threshold for no objective function value improvement, cf. "Machine-learning-based global optimization" section	10
ε_{TR}	Termination threshold for local parameter tuning stage, cf. section "Final tuning" section	10^{-3}

Table 1. Proposed algorithm: control parameters.

1. Input parameters:
   - Definition of the objective function U (cf. Design task formulation);
   - Design space X (interval $[\boldsymbol{l}\ \boldsymbol{u}]$, where $\boldsymbol{l}$ and $\boldsymbol{u}$ are lower and upper bounds for designable parameters);
   - Control parameters (N_r, N_i, E_{max}, termination thresholds ε and $N_{no\_improve}$, cf. Table 1);
2. General N_r random observables and perform the FGSA procedure (cf. Fast global sensitivity analysis) to determine surrogate model domain dimensionality N_d and the spanning vectors $\boldsymbol{e}_k$;
3. Define dimensionality-reduced surrogate model domain X_d (cf. Dimensionality-reduced model domain
4. Construct initial surrogate model $\boldsymbol{s}^{(0)}(\boldsymbol{x})$, cf. Initial surrogate (also, Fig. 8);
5. Set $i = 0$;
6. Obtain infill point $\boldsymbol{x}^{(i+1)}$ by solving (12) using the PSO algorithm:
   $$\boldsymbol{x}^{(i+1)} = \arg\min_{\boldsymbol{x}\in X_d} U_S(\boldsymbol{x}, \boldsymbol{s}^{(i)}(\boldsymbol{x}))$$
7. Update the dataset: $\{\boldsymbol{x}_B^{(k)}, \boldsymbol{R}(\boldsymbol{x}_B^{(k)})\}_{k=1,\ldots,2NiNd+i}$, where $\boldsymbol{x}_B^{(2NiNd+i)} = \boldsymbol{x}^{(i)}$ for $i = 1, 2, \ldots$.
8. Set $i = i + 1$;
9. Construct the surrogate model $\boldsymbol{s}^{(i)}(\boldsymbol{x})$ using the updated dataset;
10. **if** $||\boldsymbol{x}^{(i)} - \boldsymbol{x}^{(i-1)}|| < \varepsilon$ OR no objective function improvement for $N_{no\_improve}$ iterations
    Go to 11;
    end
11. Go to 6;
12. Perform local tuning over the original parameter space X, cf. Final tuning
    $$\boldsymbol{x}^* = \arg\min_{\boldsymbol{x}\in X} U(\boldsymbol{x})$$
    The starting point is vector $\boldsymbol{x}^{(i)}$ found during the global search stage;
13. Return $\boldsymbol{x}^*$;

Fig. 9. Pseudocode of the proposed procedure. The essential part of the algorithm is dimensionality-reduced surrogate established in the domain defined using the proposed fast global sensitivity analysis scheme.

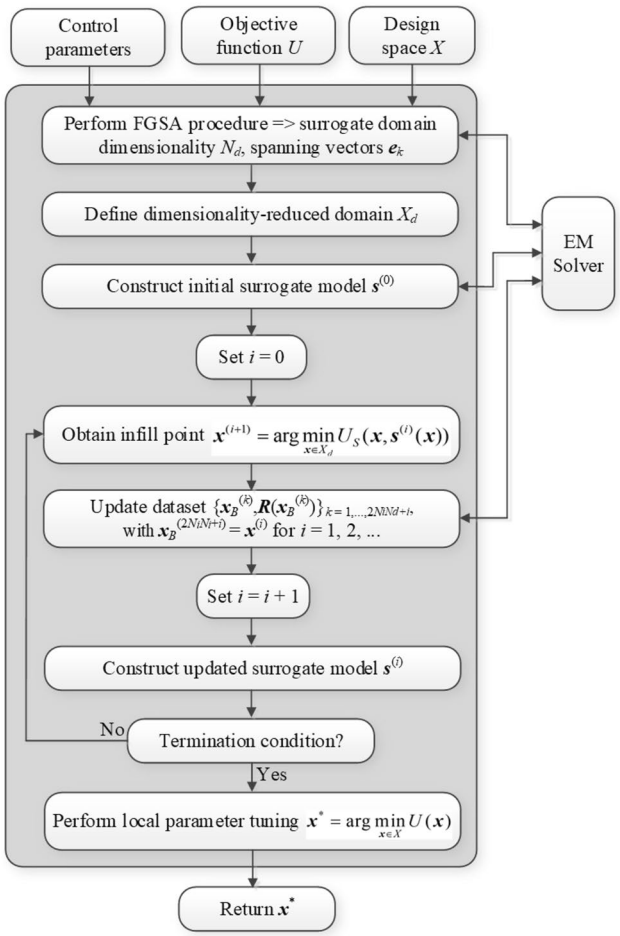

Fig. 10. Flow diagram of the FGSA-based optimization procedure.

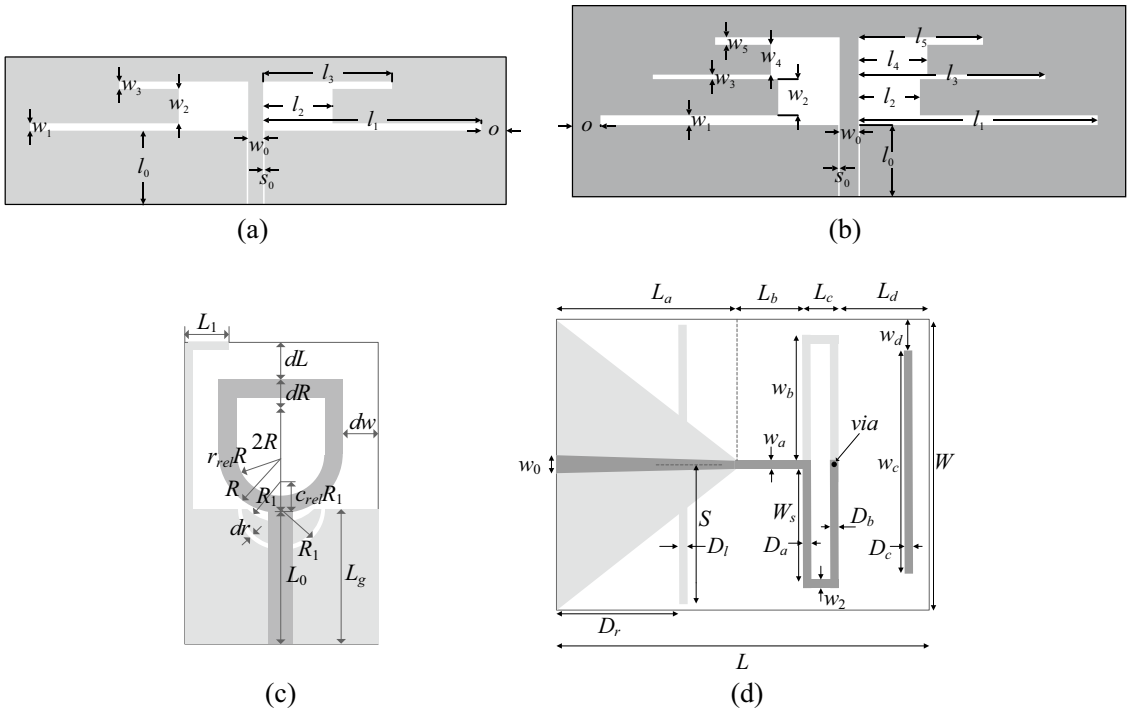

Fig. 11. Test cases: Antennas I, II, III, and IV[112–115]. Antennas geometries are shown in panels (**a**) through (**d**), respectively. The ground planes for Antennas III and IV are marked using the light-shade grey.

Parameter	Antenna structure			
	Antenna I	**Antenna II**	**Antenna III**	**Antenna IV**
Substrate	RO4350 ($\varepsilon_r = 3.5$, $h = 0.76$ mm)	RO4350 ($\varepsilon_r = 3.5$, $h = 0.76$ mm)	RF-35 ($\varepsilon_r = 3.5$, $h = 0.762$ mm)	RO4003 ($\varepsilon_r = 3.38$, $h = 1.5$ mm)
Design parameters[$]	$\boldsymbol{x} = [l_1\ l_2\ l_3\ w_1\ w_2\ w_3]^T$	$\boldsymbol{x} = [l_1\ l_2\ l_{3r}\ l_4\ l_{5r}\ w_1\ w_2\ w_3\ w_4\ w_5]^T$	$\boldsymbol{x} = [L_0\ dR\ R\ r_{rel}\ dL\ dw\ Lg\ L_1\ R_1\ dr\ c_{rel}]^T$	$\boldsymbol{x} = [L_a\ L_b\ L_c\ L_d\ W\ w_a\ D_a\ D_b\ D_c\ D_{lr}\ D_{rr}\ S_r\ w_{br}\ w_{cr}]^T$
Other parameters[$]	$l_0 = 30$, $w_0 = 3$, $s_0 = 0.15$, $o = 5$	$l_3 = l_{3r}l_1$ and $l_5 = l_{5r}l_3$; $l_0 = 30$, $w_0 = 3$, $s_0 = 0.15$, $o = 5$	$w_0 = 1.7$	$D_l = D_{lr}L_a$, $D_r = D_{rr}L_a$, $S = S_rW$, $w_b = w_{br}W/2$, $w_c = w_{cr}W$, $w_0 = 3.4$
EM model	CST Microwave Studio	CST Microwave Studio	CST Microwave Studio	CST Microwave Studio
Target operating frequencies [GHz]	2.45 GHz 5.3 GHz	2.45 GHz 3.6 GHz 5.3 GHz	3.1–10.6 GHz	2.5 GHz
Design goals	Minimize reflection at all operating frequencies	Minimize reflection at all operating frequencies	Minimize reflection within the entire UWB band	Maximize realized gain in ± 100 MHz bandwidth centred at $\boldsymbol{f}_0$; Constraint: $\lvert S_{11}\rvert \leq -10$ dB at the same bandwidth
Parameter space X	$\boldsymbol{l} = [15\ 3\ 0.35\ 0.2\ 1.8\ 0.5]^T$ $\boldsymbol{u} = [50\ 12\ 0.85\ 1.5\ 4.3\ 2.7]^T$	$\boldsymbol{l} = [20\ 3\ 0.6\ 3\ 0.6\ 0.2\ 0.2\ 0.2\ 0.2\ 0.2]^T$ $\boldsymbol{u} = [50\ 5\ 0.85\ 5\ 0.85\ 2.2\ 4.2\ 2.2\ 4.2\ 2.2]^T$	$\boldsymbol{l} = [4.0\ 0.0\ 3.0\ 0.1\ 0.0\ 0.0\ 4.0\ 0.0\ 2.0\ 0.2\ 0.2]^T$ $\boldsymbol{u} = [15.0\ 6.0\ 8.0\ 0.9\ 5.0\ 8.0\ 15.0\ 6.0\ 5.0\ 1.0\ 0.9]^T$	$\boldsymbol{l} = [15\ 5\ 1\ 15\ 25\ 0.5\ 1\ 1.5\ 1.5\ 0.05\ 0.4\ 0.5\ 0.5\ 0.5]^T$ $\boldsymbol{u} = [35\ 25\ 8\ 40\ 60\ 2.5\ 3.0\ 4.5\ 4.5\ 0.25\ 0.9\ 1.0\ 1.0\ 1.0]^T$

Table 2. Verification antenna structures. [$]Dimensions in mm, except relative one (with subscript r), which are unitless.

parts of this section are arranged as follows: "Test cases" section outlines the test cases. The experimental setup and results are presented in "Results" section, followed by a discussion of the results in "Discussion" section.

Test cases

Our verification antenna set consists of four microstrip structures:

- Dual-band uniplanar dipole fed by a coplanar-waveguide (CPW) (Antenna I)[112];
- CPW-fed triple-band dipole (Antenna II)[113];
- Compact ultra-wideband (UWB) monopole (Antenna III)[114];
- Quasi-Yagi antenna with integrated balun (Antenna IV)[115].

The antenna geometries can be found in Fig. 11. Table 2 puts together data on material parameters, design variables, target center frequencies, and lower and upper bound vectors $\boldsymbol{l}$ and $\boldsymbol{u}$ defining the original design variable

Algorithm	Algorithm type	Setup
This work	FGSA-based surrogate-assisted machine-learning framework with dimensionality reduction	Control parameters: $N_r = 50$, $N_i = 20$, $E_{max} = 20\%$, $\varepsilon = 10^{-2}$, $N_{no\_improve} = 20$, $\varepsilon_{TR} = 10^{-3}$ (see Table 1 for explanation of terms)
I	Particle swarm optimizer (PSO)	Swarm size $N = 10$, standard control parameters ($\chi = 0.73$, $c_1 = c_2 = 2.05$); number of iterations set to 50 (version I) and 100 (version II)
II	Trust-region gradient based optimizer[108]	Random initial design, response gradients estimated using finite differentiation, termination criteria based on convergence in argument and reduction of the trust region size[108]
III	Machine-learning procedure	Algorithm setup: Initial surrogate set up to ensure relative RMS error not higher than 20% with the maximum number of training samples equal to 400 Algorithm operates in the original parameter space (no dimensionality reduction) Infill criterion: minimization of the predicted objective function

Table 3. Benchmark algorithms.

space X. The EM models are prepared in CST Microwave Studio[116]. Frequency characteristics are computed using the time-domain solver. For Antennas I and II, the design goal is matching improvement at individual (target) frequencies. Antenna III is optimized for best impedance matching within the UWB band (3.1–10.6 GHz), whereas the goal for Antenna IV is maximization of the in-band gain within 200 MHz band centred at 2.5 GHz.

The presented optimization problems are intricate due to the nonlinearity of antenna responses and broad geometry parameter ranges, but also design variable space dimensionality (from six variables for Antenna I to fourteen for Antenna IV). The average upper-to-lower bound ratio is 4.2, 8.4, 2.8, and 2.6 for Antennas I through IV; however, for Antenna III, the parameters with the zero lower bound have been excluded from calculations.

Results

The arrangements used for the suggested framework and the benchmark techniques are encapbulated in Table 3. Our algorithm is run using the default values for the control variables, see Table 1. The first benchmark algorithm (Algorithm I) is perhaps the most popular (and exemplary) nature-inspired routine, i.e., particle swarm optimizer (PSO)[106]. It is run in two versions, with the computational budget of 500 (Version I) and 1,000 (Version II) objective function evaluations. Note that these budgets are low for population-based methods yet considerable given that PSO directly optimizes EM simulation models. The second routine (Algorithm II) is a multiple-start gradient procedure (here, we use the trust-region algorithm, similar to that outlined in "Final tuning" section). It is employed to showcase that the verification problems considered here are multimodal. The third benchmark algorithm (Algorithm III) is a machine-learning procedure employing the same type of surrogate model (kriging) and the same infill criterion as the proposed technique; however, it operates in the original parameter space of full dimensionality. This algorithm is included to showcase the advantages of dimensionality reduction fully.

The results for Antennas I, II, III, and IV are compiled in Tables 4 through 7, respectively. All algorithms were executed ten times each, and the data in the tables represent the mean values of the performance indicators (merit function value and its standard deviation, CPU cost). Additionally, the success rate is reported, indicating the number of runs (out of ten) for which the given algorithm successfully identified a design with operating frequencies sufficiently close to the target values. Furthermore, Figs. 12, 13, 14 and 15 depict the antenna responses upon completing the global search stage and at the final designs for representative algorithm runs.

Discussion

In this section, we analyze the numerical data presented in Tables 4, 5, 6 and 7 and provide a summary of the performance of the suggested algorithm. We also discuss its comparison with benchmark methods. The following observations emerge from our analysis:

Optimization algorithm	Performance figure			
	Average objective function value (dB)	Standard deviation of objective function (dB)	Computational cost[$]	Success rate[#]
Algorithm I: PSO (50 iterations)	− 18.2	3.2	500	9/10
Algorithm I: PSO (100 iterations)	− 19.3	2.7	1000	10/10
Algorithm II: Trust-region gradient-based algorithm	− 13.5	4.3	84.2	6/10
Algorithm III: Machine learning operating in the original parameter space X	− 20.7	1.3	457.8	10/10
Proposed algorithm	− 20.6	1.8	221.8	10/10

Table 4. Results for Antenna I. [$]The cost expressed in terms of the number of EM simulations of the antenna structure under design. [#]Number of algorithms runs at which the operating frequencies were allocated in the vicinity of the target frequencies.

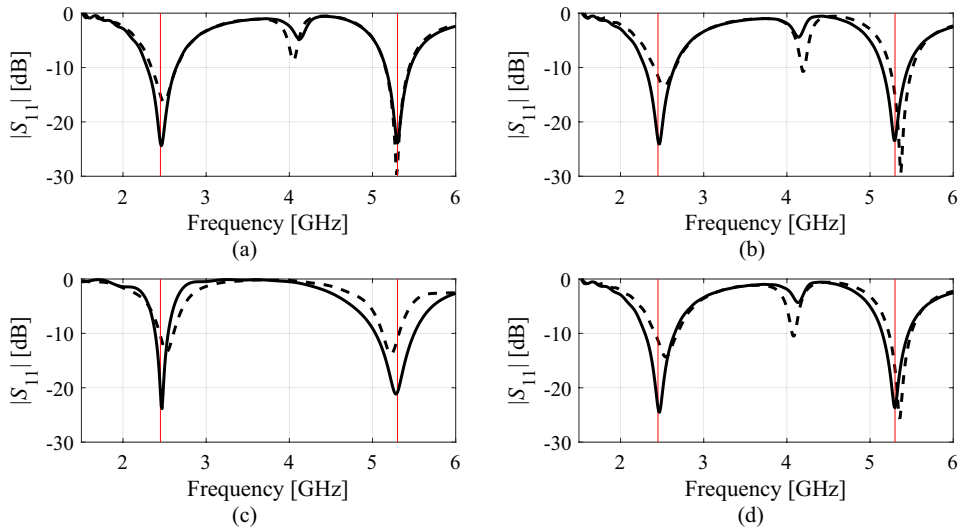

Fig. 12. Antenna I reflection characteristics at the designs found using the proposed algorithm: starting point $\boldsymbol{x}^{(0)}$ found through global search (- - -), final design (—). The pictures (**a**)–(**d**) show results for four exemplary runs. Target center frequencies denoted as vertical lines.

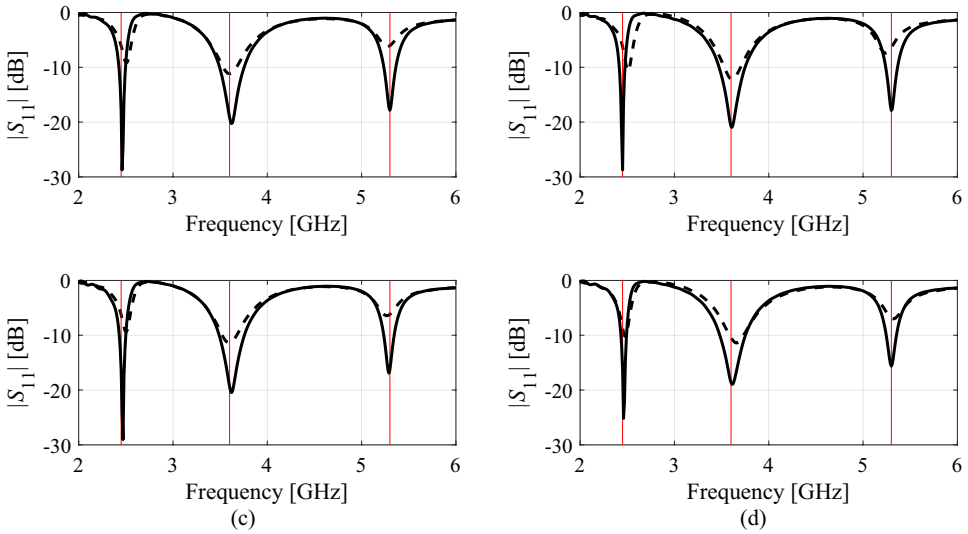

Fig. 13. Antenna II reflection characteristics at the designs found using the proposed algorithm: starting point $\boldsymbol{x}^{(0)}$ found through global search (- - -), final design (—). The pictures (**a**)–(**d**) show results for four exemplary runs. Target center frequencies denoted as vertical lines.

- *Global optimization capability and design reliability* The numerical data indicates that the proposed optimization framework achieves a perfect success rate, i.e., it is capable of yielding acceptable design at each run (i.e., 10/10). Its operation is consistent for all four antenna structures. Meanwhile, the results for Algorithm II (multiple-start gradient search) corroborate that all considered tasks are multimodal: the success rate is only 6/10, 4/10, 5/10, and 1/10 for Antennas I through IV, respectively. Algorithm I (PSO) performs better; however, its average success rate is only 8/10 for the budget of 500 EM analyses. It is improved but still not perfect for all antennas for the budget of 1,000, which—as expected—indicates that nature-inspired search normally requires much higher number of objective function evaluations to ensure success. The machine learning framework (Algorithm III) outperforms PSO, and its success rate is as good as that of the proposed technique (10/10 for all problems but Antenna III). Yet, due to operating in the full-dimensionality parameter spaces, its computational cost is higher. The competitive reliability-wise performance of the proposed procedure is also reflected in the standard deviation of the objective function values reported in Tables 4, 5, 6 and 7. As it can be observed, standard deviation is the lowest for our algorithm (only matched by Algorithm II for some test cases), which is another indication of excellent repeatability of results.

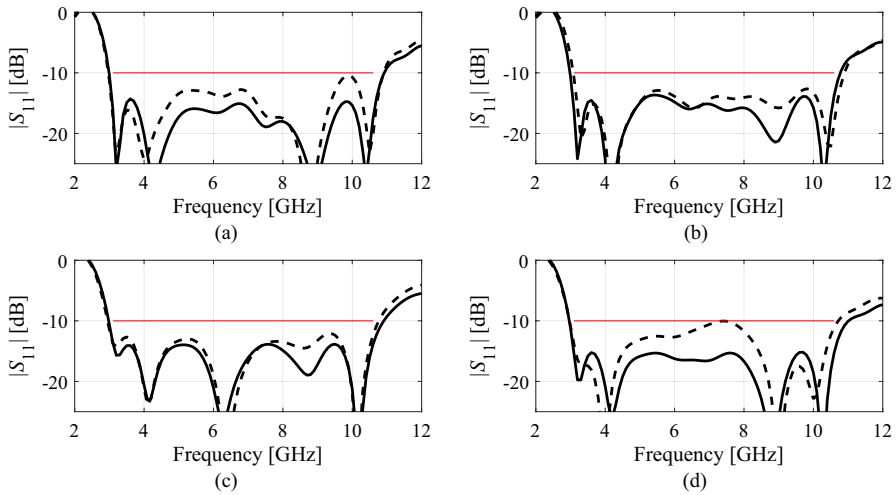

Fig. 14. Antenna III reflection characteristics at the designs found using the proposed algorithm: starting point $\boldsymbol{x}^{(0)}$ found through global search (- - -), final design (—). The pictures (**a**)–(**d**) show results for four exemplary runs. Target operating bandwidth marked using the horizontal line at the acceptance threshold of – 10 dB.

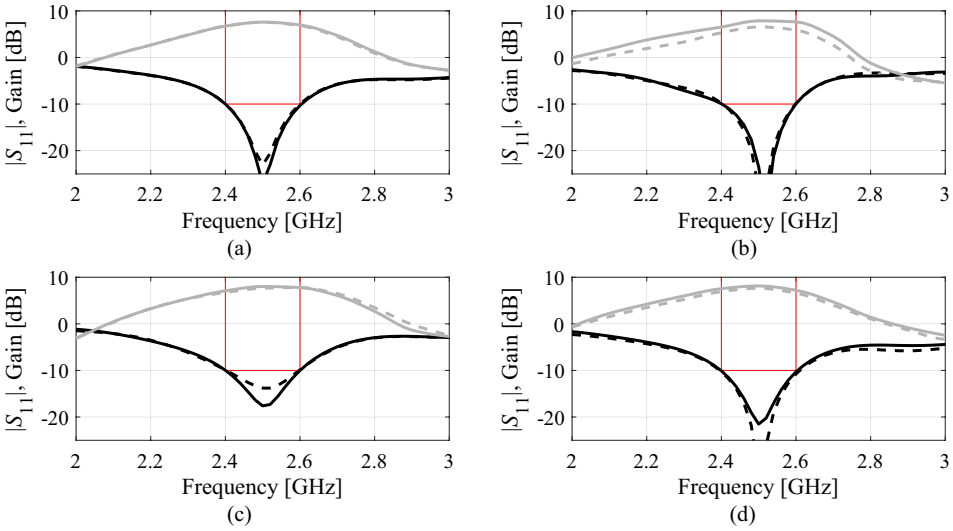

Fig. 15. Antenna IV reflection (black) and realized gain (gray) characteristics at the designs found using the proposed algorithm: starting point $\boldsymbol{x}^{(0)}$ found through global search (- - -), final design (—). The pictures (**a**)–(**d**) show results for four exemplary runs. Vertical and horizontal lines mark the target bandwidth 2.4–2.6 GHz, and the intended impedance matching bandwidth level of – 10 dB.

Optimization algorithm	Performance figure			
	Average objective function value (dB)	Standard deviation of objective function (dB)	Computational cost[$]	Success rate[#]
Algorithm I: PSO (50 iterations)	– 10.8	4.1	500	5/10
Algorithm I: PSO (100 iterations)	– 13.8	3.0	1000	8/10
Algorithm II: Trust-region gradient-based algorithm	– 7.8	4.8	105.8	4/10
Algorithm III: Machine learning operating in the original parameter space X	– 13.5	3.5	470.0	10/10
Proposed algorithm	– 15.4	2.4	303.7	10/10

Table 5. Results for Antenna II. [$]The cost expressed in terms of the number of EM simulations of the antenna structure under design. [#]Number of algorithms runs at which the operating frequencies were allocated in the vicinity of the target frequencies.

Optimization algorithm	Performance figure			
	Average objective function value (dB)	Standard deviation of objective function (dB)	Computational cost[$]	Success rate[#]
Algorithm I: PSO (50 iterations)	− 12.3	2.8	500	9/10
Algorithm I: PSO (100 iterations)	− 12.6	2.0	1000	10/10
Algorithm II: Trust-region gradient-based algorithm	− 7.8	3.2	99.2	5/10
Algorithm III: Machine learning operating in the original parameter space X	− 11.8	1.4	471.6	9/10
Proposed algorithm	− 13.2	1.2	308.1	10/10

Table 6. Results for Antenna III. [$]The cost expressed in terms of the number of EM simulations of the antenna structure under design. [#]Number of algorithms runs at which the maximum in-band matching was reduced below − 10 dB.

Optimization algorithm	Performance figure			
	Average objective function value (dB)[&]	Standard deviation of objective function (dB)	Computational cost[$]	Success rate[#]
Algorithm I: PSO (50 iterations)	6.1	0.7	500	9/10
Algorithm I: PSO (100 iterations)	6.8	0.5	1000	10/10
Algorithm II: Trust-region gradient-based algorithm	− 1.1	2.5	144.3	1/10
Algorithm III: Machine learning operating in the original parameter space X	7.9	0.3	583.3	10/10
Proposed algorithm	8.0	0.2	370.4	10/10

Table 7. Results for Antenna IV. [&]The values reported in the table refer to the realized gain at the target operating frequency of 2.5 GHz. [$]The cost expressed in terms of the number of EM simulations of the antenna structure under design. [#]Number of algorithms runs at which the operating frequencies were allocated in the vicinity of the target frequency.

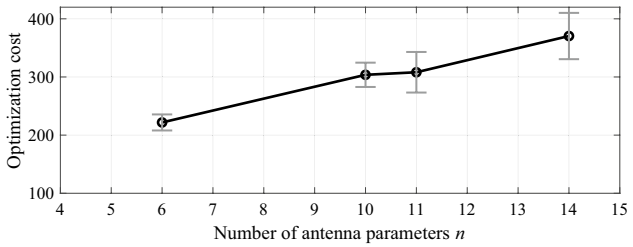

Fig. 16. Average CPU cost of the proposed global search framework as a function the number of antenna parameters. The cost is presented as the number of EM analyses. Vertical bars showcase standard deviation of the running cost computed based on ten independent runs.

- *Design quality* The objective function value is employed here as the design quality metric. For Antennas I through III, it is the maximum level of in-band $|S_{11}|$. For Antenna IV it is the end-fire realized gain at the center frequency. The numerical results of Tables 4, 5, 6 and 7 demonstrate that our algorithm produces designs of the highest quality in comparison to all benchmark techniques. The second best method is Algorithm III (machine learning working in the original design variable space X), for which the design quality is essentially the same as for the proposed approach for Antennas I and IV. Multiple-start gradient optimization produces inferior results on the average because for most runs, the search process is stuck in poor local optima. The performance of the PSO algorithm improves between the budget of 500 and 1,000 objective function evaluations, which, again, corroborates the previous observation that this sort of methods normally require significantly higher budgets to become reliable optimizers. It is especially noticeable for Antenna IV, where machine learning frameworks allow for achieving end-fire gains better by over 1 dB than the PSO algorithm.
- *CPU efficiency* The CPU efficiency of the presented framework is excellent, especially keeping in mind its global search ability. The average CPU expenses associated with the algorithm are 300 EM analyses of the respective device per run, and the complexity scales almost linearly w.r.t. the number of antenna design variables (cf. Figure 16). Clearly, our procedure is more expensive than local optimization; however, in this

work, we are concerned with comparison of the efficiency of global search procedures. When compared with Algorithm III, the expenses incurred by the proposed approach are forty percent lower on the average. Assuming that the minimum budget of Algorithm I necessary to ensure that its performance is more or less comparable to machine learning routines is 2,000 objective function calls, the cost of our technique would be then lower by 85 percent.

- Comparison with the machine learning procedure operating over the original space X (Algorithm III) indicates a major role of dimensionality reduction in enhancing the dependability and cost efficiency of the search process. It should be noted that both the cost of FGSA and final tuning have been included into the overall expenses. Yet, even with these extra costs, our technique offers over forty percent savings over Algorithm III. Also, for some of the test cases (Antennas II and III) it yields designs of higher quality. Operating in lower-dimensionality domain dramatically reduces the cost of setting up surrogate model while improving its predictive power. For the particular examples considered in this section, and surrogate model domain dimensionalities are $N_d = 3$ for Antenna I, $N_d = 5$ for Antenna II, $N_d = 4$ for Antenna III, and $N_d = 5$ for Antenna IV, which corresponds to reduction factors of 2.0, 2.0, 2.8, and 2.8, respectively with the average of 2.4.

The observations formulated above indicate that the proposed machine learning framework does exhibit global search capability, and offers consistent performance for a variety of test cases that include antenna optimization under different scenarios (multi-band, broadband, high gain). In a large part, excellent reliability and repeatability of results, as well as low computational cost, are possible due to the involvement of global sensitivity analysis, and the resulting dimensionality reduction. The latter allows for constructing decent-quality surrogate models at low CPU cost when compared to what is required in full-dimensional parameter spaces. This carries over to improved efficacy and the quality of the designs generated by the presented algorithm. Further, the proposed framework has just a few control variables. Apart from those related to the termination criteria (which, in fact, decide upon the resolution of the optimization process), there are only three parameters, the values of which are not critical, as shown by utilizing identical setup for all verification antenna structures.

Conclusion

This paper introduced an innovative technique for global optimization of antenna structures. The presented approach capitalizes on dimensionality reduction realized through dedicated fast global sensitivity analysis (FGSA) procedure. FGSA allows us to determine the directions within the parameters space that are important for their effects on antenna responses. Restricting the global search stage to the sub-space spanned by a few directions facilitates the construction of fast replacement models (surrogates), working as predictors within the machine learning loop. The latter employs predicted objective function improvement as an infill criterion and enables rapid identification of the parameter space regions encapsulating high-quality designs. The final design is obtained using auxiliary local (gradient-based) tuning over the original parameter space. The incorporation of the aforementioned tools leads to a framework that operates consistently and reliably while exhibiting low computational cost. These features have been corroborated through extensive numerical validation that involves four antenna structures of distinct characteristics. The associated optimization tasks are challenging both in terms multimodality, nonlinearity of antenna responses, as well as large parameter spaces (dimensionality from six to fourteen, broad spectra of evaluation frequencies, and wide ranges of designable parameters). Notwithstanding, the proposed approach demonstrated consistency and perfect success rate over multiple algorithm runs, but also competitive performance w.r.t. the benchmark methods. Meanwhile, its computational efficiency is significantly better than that of nature-inspired methods directly handling the EM antenna models. The presented machine learning framework is generic, i.e., it does not make any underlying assumptions about the antenna under design or its characteristics. It is easy to set up due to a small number of control parameters, and relatively straightforward to implement. Consequently, it might become an attractive alternative for existing methods whenever global search capability is required at reasonable computational expenses. One of the goals of the future work is to investigate the effects of selecting the dimensionality of the reduced domain. At the qualitative level, it is expected that reducing dimensionality (i.e., reducing the threshold $C_{\min}$) would expedite the optimization process while being detrimental to the reliability. Whereas, increasing the dimensionality might further improve the design quality while increasing the running time.

Data availability

The datasets used and/or analyzed during the current study available from the corresponding author on reasonable request.

Received: 18 June 2024; Accepted: 9 September 2024
Published online: 16 September 2024

References

1. Zhang, Y., Deng, J., Li, M., Sun, D. & Guo, L. A MIMO dielectric resonator antenna with improved isolation for 5G mm-wave applications. *IEEE Antennas Wirel. Propag. Lett.* **18**(4), 747–751 (2019).
2. Wen, S. & Dong, Y. A low-profile wideband antenna with monopolelike radiation characteristics for 4G/5G indoor micro base station application. *IEEE Antennas Wirel. Propag. Lett.* **19**(12), 2305–2309 (2020).
3. Jha, K. R., Bukhari, B., Singh, C., Mishra, G. & Sharma, S. K. Compact planar multistandard MIMO antenna for IoT applications. *IEEE Trans. Antennas Propag.* **66**(7), 3327–3336 (2018).
4. Lin, X. *et al.* Ultrawideband textile antenna for wearable microwave medical imaging applications. *IEEE Trans. Antennas Propag.* **68**(6), 4238–4249 (2020).

5. Kapusuz, K. Y., Berghe, A. V., Lemey, S. & Rogier, H. Partially filled half-mode substrate integrated waveguide leaky-wave antenna for 24 GHz automotive radar. *IEEE Antennas Wirel. Propag. Lett.* **20**(1), 33–37 (2021).
6. Mansour, M. M. & Kanaya, H. High-efficient broadband CPW RF rectifier for wireless energy harvesting. *IEEE Microw. Wirel. Compon. Lett.* **29**(4), 288–290 (2019).
7. Erman, F., Koziel, S., Hanafi, E., Soboh, R. & Szczepanski, S. Miniaturized metal-mountable U-shaped inductive-coupling-fed UHF RFID tag antenna with defected microstrip surface. *IEEE Access* **10**, 47301–47308 (2022).
8. He, Y., Yue, Y., Zhang, L. & Chen, Z. N. A dual-broadband dual-polarized directional antenna for all-spectrum access base station applications. *IEEE Trans. Antennas Propag.* **69**(4), 1874–1884 (2021).
9. Sun, L., Li, Y., Zhang, Z. & Feng, Z. Wideband 5G MIMO antenna with integrated orthogonal-mode dual-antenna pairs for metal-rimmed smartphones. *IEEE Trans. Antennas Propag.* **68**(4), 2494–2503 (2020).
10. Sung, Y. Simple slot antenna with polarization diversity. *IEEE Antennas Wirel. Propag. Lett.* **21**(4), 690–694 (2022).
11. Xu, H.-X. *et al.* Polarization-insensitive metalens and its applications to reflectarrays with polarization diversity. *IEEE Trans. Antennas Propag.* **70**(3), 1895–1905 (2022).
12. Hynes, C. G. & Vaughan, R. G. Conical monopole antenna with integrated tunable notch filters. *IEEE Antennas Wirel. Propag. Lett.* **19**(12), 2398–2402 (2020).
13. Rabbani, M. S., Churm, J. & Feresidis, A. P. Continuous beam-steering low-loss millimeter-wave antenna based on a piezoelectrically actuated metasurface. *IEEE Trans. Antennas Propag.* **70**(4), 2439–2449 (2022).
14. Farahat, A. E., Hussein, K. F. A. & El-Hassan, M. A. Design methodology of multiband printed antennas for future generations of mobile handsets. *IEEE Access* **10**, 75918–75931 (2022).
15. Chen, C. A compact wideband endfire filtering antenna inspired by a uniplanar microstrip antenna. *IEEE Antennas Wirel. Propag. Lett.* **21**(4), 853–857 (2022).
16. Chen, Z. *et al.* Compact wideband circularly polarized loop antenna based on dual common and differential modes. *IEEE Antennas Wirel. Propag. Lett.* **21**(8), 1567–1571 (2022).
17. Nagaraju, D. & Verma, Y. K. A compact conformal stub-loaded long slot leaky-wave antenna with wide beamwidth. *IEEE Antennas Wirel. Propag. Lett.* **20**(6), 953–957 (2021).
18. Sun, L., Li, Y. & Zhang, Z. Wideband dual-polarized endfire antenna based on compact open-ended cavity for 5G Mm-wave mobile phones. *IEEE Trans. Antennas Propag.* **70**(3), 1632–1642 (2022).
19. Chen, X., Tang, M.-C., Yi, D. & Ziolkowski, R. W. Wideband, compact antennas with interdigitated magnetic-based near-field resonant parasitic elements. *IEEE Trans. Antennas Propag.* **69**(8), 5036–5041 (2021).
20. Cicchetti, R., Cicchetti, V., Faraone, A., Foged, L. & Testa, O. A compact high-gain wideband lens Vivaldi antenna for wireless communications and through-the-wall imaging. *IEEE Trans. Antennas Propag.* **69**(6), 3177–3192 (2021).
21. Liu, Y. & Yagoub, M. C. E. Compact omnidirectional millimeter-wave antenna array fed in series by a novel feed network. *IEEE Trans. Antennas Propag.* **69**(11), 7604–7612 (2021).
22. Hu, H. *et al.* Compact planar inverted-F antenna for MicroSats omnidirectional communications. *IEEE Antennas Wirel. Propag. Lett.* **20**(2), 160–164 (2021).
23. Podilchak, S. K., Johnstone, J. C., Caillet, M., Clénet, M. & Antar, Y. M. M. A compact wideband dielectric resonator antenna with a meandered slot ring and cavity backing. *IEEE Antennas Wirel. Propag. Lett.* **15**, 909–913 (2016).
24. Hu, W., Yin, Y., Yang, X. & Fei, P. Compact multiresonator-loaded planar antenna for multiband operation. *IEEE Trans. Antennas Propag.* **61**(5), 2838–2841 (2013).
25. Haq, M. A., Koziel, S. & Cheng, Q. S. Miniaturization of wideband antennas by means of feed line topology alterations. *IET Microw. Antennas Propag.* **12**(13), 2128–2134 (2018).
26. Ding, Z., Jin, R., Geng, J., Zhu, W. & Liang, X. Varactor loaded pattern reconfigurable patch antenna with shorting pins. *IEEE Trans. Antennas Propag.* **67**(10), 6267–6277 (2019).
27. Zhu, S., Liu, H., Wen, P., Chen, Z. & Xu, H. Vivaldi antenna array using defected ground structure for edge effect restraint and back radiation suppression. *IEEE Antennas Wirel. Propag. Lett.* **19**(1), 84–88 (2020).
28. Gallardo, D., Monasterio, D., Finger, R., Mena, F. P. & Bronfman, L. A compact metamaterial-based antenna for multiband phased array applications. *IEEE Trans. Antennas Propag.* **69**(12), 8872–8877 (2021).
29. Priya, S., Dwari, S., Kumar, K. & Mandal, M. K. Compact self-quadruplexing SIW cavity-backed slot antenna. *IEEE Trans. Antennas Propag.* **67**(10), 6656–6660 (2019).
30. Li, W.-Y., Chung, W., Hsiao, F.-R., Li, T.-L., Kao, T.-H. & Huang, M.-C. Compact multi-layer handset phone 13.56 MHz NFC antenna design by novel laser-induced thin-film antenna (LITA) technologies. In *International Symposium on. Antennas and Propagation (ISAP)* 26–27 (2016).
31. Iqbal, A., Al-Hasan, M., Mabrouk, I. B. & Nedil, M. Ultracompact quarter-mode substrate integrated waveguide self-diplexing antenna. *IEEE Antennas Wirel. Propag. Lett.* **20**(7), 1269–1273 (2021).
32. Zhang, Y., Yang, W., Xue, Q., Huang, J. & Che, W. Broadband dual-polarized differential-fed filtering antenna array for 5G millimeter-wave applications. *IEEE Trans. Antennas Propag.* **70**(3), 1989–1998 (2022).
33. Ullah, U., Al-Hasan, M., Koziel, S. & Ben Mabrouk, I. EM-driven size reduction and multi-criterial optimization of broadband circularly-polarized antennas using Pareto front traversing and design extrapolation. *Sci. Rep.* **12**, 9877 (2022).
34. Koziel, S. & Pietrenko-Dabrowska, A. On EM-driven size reduction of antenna structures with explicit constraint handling. *IEEE Access* **9**, 165766–165772 (2021).
35. Chen, M.-N., Lu, W.-J., Wang, L.-J., Yang, M. & Zhu, L. Design approach to a novel planar bisensing circularly polarized antenna. *IEEE Trans. Antennas Propag.* **67**(11), 6839–6846 (2019).
36. Cuevas, M., Pizarro, F., Leiva, A., Hermosilla, G. & Yunge, D. Parametric study of a fully 3D-printed dielectric resonator antenna loaded with a metallic cap. *IEEE Access* **9**, 73771–73779 (2021).
37. Li, X. & Luk, K. M. The grey wolf optimizer and its applications in electromagnetics. *IEEE Trans. Antennas Prop.* **68**(3), 2186–2197 (2020).
38. Luo, X., Yang, B. & Qian, H. J. Adaptive synthesis for resonator-coupled filters based on particle swarm optimization. *IEEE Trans. Microw. Theory Tech.* **67**(2), 712–725 (2019).
39. Majumder, A., Chatterjee, S., Chatterjee, S., Sinha Chaudhari, S. & Poddar, D. R. Optimization of small-signal model of GaN HEMT by using evolutionary algorithms. *IEEE Microw. Wirel. Compon. Lett.* **27**(4), 362–364 (2017).
40. Liang, S. *et al.* Sidelobe reductions of antenna arrays via an improved chicken swarm optimization approach. *IEEE Access* **8**, 37664–37683 (2020).
41. Tang, M., Chen, X., Li, M. & Ziolkowski, R. W. Particle swarm optimized, 3-D-printed, wideband, compact hemispherical antenna. *IEEE Antennas Wirel. Propag. Lett.* **17**(11), 2031–2035 (2018).
42. Liu, F., Liu, Y., Han, F., Ban, Y.-L. & Jay Guo, Y. Synthesis of large unequally spaced planar arrays utilizing differential evolution with new encoding mechanism and Cauchy mutation. *IEEE Trans. Antennas Propag.* **68**(6), 4406–4416 (2020).
43. Li, W., Zhang, Y. & Shi, X. Advanced fruit fly optimization algorithm and its application to irregular subarray phased array antenna synthesis. *IEEE Access* **7**, 165583–165596 (2019).
44. Al-Azza, A. A., Al-Jodah, A. A. & Harackiewicz, F. J. Spider monkey optimization: A novel technique for antenna optimization. *IEEE Antennas Wirel. Propag. Lett.* **15**, 1016–1019 (2016).

45. Afsari, A., Abbosh, A. M. & Rahmat-Samii, Y. Adaptive beamforming by compact arrays using evolutionary optimization of Schelkunoff polynomials. *IEEE Trans. Antennas Propag.* **70**(6), 4485–4497 (2022).
46. Zheng, T. *et al.* IWORMLF: Improved invasive weed optimization with random mutation and Lévy flight for beam pattern optimizations of linear and circular antenna arrays. *IEEE Access* **8**, 19460–19478 (2020).
47. Genovesi, S., Mittra, R., Monorchio, A. & Manara, G. Particle swarm optimization for the design of frequency selective surfaces. *IEEE Antennas Wirel. Propag. Lett.* **5**, 277–279 (2006).
48. Koziel, S. & Abdullah, M. Machine-learning-powered EM-based framework for efficient and reliable design of low scattering metasurfaces. *IEEE Trans. Microw. Theory Tech.* **69**(4), 2028–2041 (2021).
49. Koziel, S. & Pietrenko-Dabrowska, A. Reliable EM-driven size reduction of antenna structures by means of adaptive penalty factors. *IEEE Trans. Antennas Propag.* **70**(2), 1389–1401 (2021).
50. Mahrokh, M. & Koziel, S. Explicit size-reduction of circularly polarized antennas through constrained optimization with penalty factor adaptation. *IEEE Access* **9**, 132390–132396 (2021).
51. Koziel, S. & Pietrenko-Dabrowska, A. Expedited acquisition of database designs for reduced-cost performance-driven modeling and rapid dimension scaling of antenna structures. *IEEE Trans. Antennas Propag.* **69**(8), 4975–4987 (2021).
52. Bora, T. C., Lebensztajn, L. & Coelho, L. D. S. Non-dominated sorting genetic algorithm based on reinforcement learning to optimization of broad-band reflector antennas satellite. *IEEE Trans. Magn.* **48**(2), 767–770 (2012).
53. Ding, D. & Wang, G. Modified multiobjective evolutionary algorithm based on decomposition for antenna design. *IEEE Trans. Antennas Propag.* **61**(10), 5301–5307 (2013).
54. Yang, C., Zhang, J. & Tong, M. S. An FFT-accelerated particle swarm optimization method for solving far-field inverse scattering problems. *IEEE Trans. Antennas Propag.* **69**(2), 1078–1093 (2021).
55. Liu, X., Du, B., Zhou, J. & Xie, L. Optimal design of elliptical beam cassegrain antenna. *IEEE Access* **9**, 120765–120773 (2021).
56. Goldberg, D. E. & Holland, J. H. *Genetic Algorithms and Machine Learning* (Springer, 1988).
57. Michalewicz, Z. *Genetic Algorithms + Data Structures = Evolution Programs* (Springer, 1996).
58. Choi, K. *et al.* Hybrid algorithm combing genetic algorithm with evolution strategy for antenna design. *IEEE Trans. Magn.* **52**(3), 1–4 (2016).
59. Wang, D., Tan, D. & Liu, L. Particle swarm optimization algorithm: An overview. *Soft Comput.* **22**, 387–408 (2018).
60. Jiang, Z. J., Zhao, S., Chen, Y. & Cui, T. J. Beamforming optimization for time-modulated circular-aperture grid array with DE algorithm. *IEEE Antennas Wirel. Propag. Lett.* **17**(12), 2434–2438 (2018).
61. Baumgartner, P. *et al.* Multi-objective optimization of Yagi–Uda antenna applying enhanced firefly algorithm with adaptive cost function. *IEEE Trans. Magn.* **54**(3), 1–4 (2018).
62. Yang, S. H. & Kiang, J. F. Optimization of sparse linear arrays using harmony search algorithms. *IEEE Trans. Antennas Propag.* **63**(11), 4732–4738 (2015).
63. Zhu, D. Z., Werner, P. L. & Werner, D. H. Design and optimization of 3-D frequency-selective surfaces based on a multiobjective lazy ant colony optimization algorithm. *IEEE Trans. Antennas Propag.* **65**(12), 7137–7149 (2017).
64. Zheng, T. *et al.* IWORMLF: Improved invasive weed optimization with random mutation and Lévy flight for beam pattern optimizations of linear and circular antenna arrays. *IEEE Access* **8**, 19460–19478 (2020).
65. Tang, W. J., Li, M. S., Wu, Q. H. & Saunders, J. R. Bacterial foraging algorithm for optimal power flow in dynamic environments. *IEEE Trans. Circuits Syst. I Regul. Pap.* **55**(8), 2433–2442 (2008).
66. Prabhakar, S. K., Rajaguru, H. & Lee, S. A framework for schizophrenia EEG signal classification with nature inspired optimization algorithms. *IEEE Access* **8**, 39875–39897 (2020).
67. Darvish, A. & Ebrahimzadeh, A. Improved fruit-fly optimization algorithm and its applications in antenna arrays synthesis. *IEEE Trans. Antennas Propag.* **66**(4), 1756–1766 (2018).
68. Oyelade, O. N., Ezugwu, A.E.-S., Mohamed, T. I. A. & Abualigah, L. Ebola optimization search algorithm: A new nature-inspired metaheuristic optimization algorithm. *IEEE Access* **10**, 16150–16177 (2022).
69. Yang, X. S. Nature-inspired optimization algorithms: challenges and open problems. *J. Comput. Sci.* **46**, 101104 (2020).
70. He, X. *et al.* Distributed evolution strategies for black-box stochastic optimization. *IEEE Trans. Parallel Distrib. Syst.* **33**(12), 3718–3731 (2022).
71. Queipo, N. V. *et al.* Surrogate-based analysis and optimization. *Progress Aerosp. Sci.* **41**(1), 1–28 (2005).
72. Easum, J. A., Nagar, J., Werner, P. L. & Werner, D. H. Efficient multi-objective antenna optimization with tolerance analysis through the use of surrogate models. *IEEE Trans. Antennas Propag.* **66**(12), 6706–6715 (2018).
73. Koziel, S. & Pietrenko-Dabrowska, A. Rapid multi-objective optimization of antennas using nested kriging surrogates and single-fidelity EM simulation models. *Eng. Comput.* **37**(4), 1491–1512 (2019).
74. de Villiers, D. I. L., Couckuyt, I. & Dhaene, T. Multi-objective optimization of reflector antennas using kriging and probability of improvement. In International Symposium on Antennas and Propagation 985–986 (2017).
75. Dong, J., Qin, W. & Wang, M. Fast multi-objective optimization of multi-parameter antenna structures based on improved BPNN surrogate model. *IEEE Access* **7**, 77692–77701 (2019).
76. Jacobs, J. P. Characterization by Gaussian processes of finite substrate size effects on gain patterns of microstrip antennas. *IET Microw. Antennas Propag.* **10**(11), 1189–1195 (2016).
77. Wu, Q., Wang, H. & Hong, W. Multistage collaborative machine learning and its application to antenna modeling and optimization. *IEEE Trans. Antennas Propag.* **68**(5), 3397–3409 (2020).
78. Forrester, A. I. J. & Keane, A. J. Recent advances in surrogate-based optimization. *Prog. Aerosp. Sci.* **45**, 50–79 (2009).
79. Couckuyt, I., Declercq, F., Dhaene, T., Rogier, H. & Knockaert, L. Surrogate-based infill optimization applied to electromagnetic problems. *Int. J. RF Microw. Computt. Aided Eng.* **20**(5), 492–501 (2010).
80. Alzahed, A. M., Mikki, S. M. & Antar, Y. M. M. Nonlinear mutual coupling compensation operator design using a novel electromagnetic machine learning paradigm. *IEEE Antennas Wirel. Prop. Lett.* **18**(5), 861–865 (2019).
81. Tak, J., Kantemur, A., Sharma, Y. & Xin, H. A 3-D-printed W-band slotted waveguide array antenna optimized using machine learning. *IEEE Antennas Wirel. Prop. Lett.* **17**(11), 2008–2012 (2018).
82. Torun, H. M. & Swaminathan, M. High-dimensional global optimization method for high-frequency electronic design. *IEEE Trans. Microw. Theory Tech.* **67**(6), 2128–2142 (2019).
83. Xia, B., Ren, Z. & Koh, C. S. Utilizing kriging surrogate models for multi-objective robust optimization of electromagnetic devices. *IEEE Trans. Magn.* **50**(2), 693–696 (2014).
84. Taran, N., Ionel, D. M. & Dorrell, D. G. Two-level surrogate-assisted differential evolution multi-objective optimization of electric machines using 3-D FEA. *IEEE Trans. Magn.* **54**(11), 1–5 (2018).
85. Lv, Z., Wang, L., Han, Z., Zhao, J. & Wang, W. Surrogate-assisted particle swarm optimization algorithm with Pareto active learning for expensive multi-objective optimization. *IEEE/CAA J. Automatica Sinica* **6**(3), 838–849 (2019).
86. Koziel, S. Low-cost data-driven surrogate modeling of antenna structures by constrained sampling. *IEEE Antennas Wirel. Prop. Lett.* **16**, 461–464 (2017).
87. Koziel, S. & Sigurdsson, A. T. Triangulation-based constrained surrogate modeling of antennas. *IEEE Trans. Antennas Prop.* **66**(8), 4170–4179 (2018).
88. Koziel, S. & Pietrenko-Dabrowska, A. Performance-based nested surrogate modeling of antenna input characteristics. *IEEE Trans. Antennas Prop.* **67**(5), 2904–2912 (2019).

89. Koziel, S. & Pietrenko-Dabrowska, A. *Performance-Driven Surrogate Modeling of High-Frequency Structures* (Springer, 2020).
90. Pietrenko-Dabrowska, A. & Koziel, S. Antenna modeling using variable-fidelity EM simulations and constrained co-kriging. *IEEE Access* **8**(1), 91048–91056 (2020).
91. Pietrenko-Dabrowska, A., Koziel, S. & Ullah, U. Reduced-cost two-level surrogate antenna modeling using domain confinement and response features. *Sci. Rep.* **12**, 4667 (2022).
92. Koziel, S. Fast simulation-driven antenna design using response-feature surrogates. *Int. J. RF Microw. CAE* **25**(5), 394–402 (2015).
93. Koziel, S. & Bandler, J. W. Reliable microwave modeling by means of variable-fidelity response features. *IEEE Trans. Microw. Theory Tech.* **63**(12), 4247–4254 (2015).
94. Pietrenko-Dabrowska, A. & Koziel, S. Generalized formulation of response features for reliable optimization of antenna input characteristics. *IEEE Trans. Antennas Propag.* **70**(5), 3733–3748 (2021).
95. Marler, R. T. & Arora, J. S. The weighted sum method for multi-objective optimization: New insights. *Struct. Multidisc. Opt.* **41**, 853–862 (2010).
96. Koziel, S., Pietrenko-Dabrowska, A. & Mahrokh, M. On decision-making strategies for improved-reliability size reduction of microwave passives: Intermittent correction of equality constraints and adaptive handling of inequality constraints. *Knowl. Based Syst.* **255**, 109745 (2022).
97. Iooss, B. & Lemaitre, P. A review on global sensitivity analysis methods. In *Uncertainty Management in Simulation-Optimization of Complex Systems* (eds Dellino, G. & Meloni, C.) 101–122 (Springer, 2015).
98. Tian, W. A review of sensitivity analysis methods in building energy analysis. *Renew. Sustain. Energy Rev.* **20**, 411–419 (2013).
99. Morris, M. D. Factorial sampling plans for preliminary computational experiments. *Technometrics* **33**, 161–174 (1991).
100. Saltelli, A. Making best use of model evaluations to compute sensitivity indices. *Compuy. Phys. Commun.* **145**, 280–297 (2002).
101. Kovacs, I., Topa, M., Buzo, A., Rafaila, M. & Pelz, G. Comparison of sensitivity analysis methods in high-dimensional verification spaces. *Acta Tecnica Napoc. Electron. Telecommun.* **57**(3), 16–23 (2016).
102. Jansen, M. J. W. Analysis of variance designs for model output. *Comput. Phys. Commun.* **117**, 25–43 (1999).
103. Beachkofski, B. & Grandhi, R. Improved distributed hypercube sampling. In *American Institute of Aeronautics and Astronautics*, paper AIAA 2002-1274 (2002).
104. Jolliffe, I. T. *Principal Component Analysis* 2nd edn. (Springer, 2002).
105. Cawley, G. C. & Talbot, N. L. C. On over-fitting in model selection and subsequent selection bias in performance evaluation. *J. Mach. Learn.* **11**, 2079–2107 (2010).
106. Vinod Chandra, S. S. & Anand, H. S. Nature inspired meta heuristic algorithms for optimization problems. *Computing* **104**, 251–269 (2022).
107. Liu, J., Han, Z., Song, W. Comparison of infill sampling criteria in kriging-based aerodynamic optimization. In *28th International Congress of the Aeronautical Sciences* 1–10 (2012).
108. Conn, A. R., Gould, N. I. M. & Toint, P. L. *Trust Region Methods, MPS-SIAM Series on Optimization* (2000).
109. Levy, H. & Lessman, F. *Finite Difference Equations* (Dover Publications Inc., 1992).
110. Broyden, C. G. A class of methods for solving nonlinear simultaneous equations. *Math. Comput.* **19**, 577–593 (1965).
111. Pietrenko-Dabrowska, A. & Koziel, S. Numerically efficient algorithm for compact microwave device optimization with flexible sensitivity updating scheme. *Int. J. RF Microw. CAE* **29**(7), e21714 (2019).
112. Chen, Y.-C., Chen, S.-Y. & Hsu, P. Dual-band slot dipole antenna fed by a coplanar waveguide. In *Proceedings of IEEE Antennas and Propagation Society International Symposium* 3589–3592 (2006).
113. Pietrenko-Dabrowska, A. & Koziel, S. Simulation-driven antenna modeling by means of response features and confined domains of reduced dimensionality. *IEEE Access* **8**, 228942–228954 (2020).
114. Alsath, M. G. N. & Kanagasabai, M. Compact UWB monopole antenna for automotive communications. *IEEE Trans. Antennas Propag.* **63**(9), 4204–4208 (2015).
115. Farran, M. *et al.* Compact quasi-Yagi antenna with folded dipole fed by tapered integrated balun. *Electronics Letters* **52**(10), 789–790 (2016).
116. CST Microwave Studio, ver. 2021, Dassault Systemes, France (2021).

Acknowledgements

The authors would like to thank Dassault Systemes, France, for making CST microwave Studio available. This work is partially supported by the Icelandic Research Fund Grant 239858 and by National Science Centre of Poland Grant 2022/47/B/ST7/00072.

Author contributions

Conceptualization, S.K., A.P.; methodology, S.K. and L.L.; data generation, S.K.; investigation, S.K. and A.P.; writing—original draft preparation, S.K. and A.P.; writing—review and editing, S.K., L.L., and A.P..; visualization, S.K. and L.L.; supervision, S.K.; project administration, S.K. and A.P.

Competing interests

The authors declare no competing interests.

Additional information

Correspondence and requests for materials should be addressed to S.K.

Reprints and permissions information is available at www.nature.com/reprints.

Publisher's note Springer Nature remains neutral with regard to jurisdictional claims in published maps and institutional affiliations.